Functional interdependence of the actin nucleator Cobl and Cobl-like in dendritic arbor development

Maryam Izadi[1], Eric Seemann[1], Dirk Schlobinski[1], Lukas Schwintzer[1], Britta Qualmann[1]*, Michael M. Kessels[1]*

[1] Institute of Biochemistry I, Jena University Hospital/Friedrich-Schiller-University Jena, 07743 Jena, Germany

* Correspondence

Britta.Qualmann@med.uni-jena.de & Michael.Kessels@med.uni-jena.de

Short title

Functional interdependence of Cobl and Cobl-like

Character count: 359396 characters incl. spaces (main text)

1

18   **Abstract**

19   Local actin filament formation is indispensable for development of the dendritic arbor of neurons. We

20   show that, surprisingly, the action of single actin filament-promoting factors was insufficient for

21   powering dendritogenesis. Instead, this process required the actin nucleator Cobl and its only

22   evolutionary distant ancestor Cobl-like acting interdependently. This coordination between Cobl-like

23   and Cobl was achieved by physical linkage by syndapin I. Syndapin I formed nanodomains at convex

24   plasma membrane areas at the base of protrusive structures and interacted with three motifs in Cobl-

25   like, one of which was Ca^{2+}/calmodulin-regulated. Consistently, syndapin I, Cobl-like's newly

26   identified N terminal calmodulin-binding site and the single Ca^{2+}/calmodulin-responsive syndapin-

27   binding motif all were critical for Cobl-like's functions. In dendritic arbor development, local

28   Ca^{2+}/CaM-controlled actin dynamics thus relies on regulated and physically coordinated interactions

29   of different F-actin formation-promoting factors and only together they have the power to bring about

30   the sophisticated neuronal morphologies required for neuronal network formation.

31

Introduction

The actin cytoskeleton is crucial for a huge variety of key processes in cell biology. Yet, only few factors were found that can promote the *de novo* formation of actin filaments (Chesarone & Goode 2009; Qualmann & Kessels, 2009). Thus, the initial idea that each of the discovered actin nucleators may be responsible for the formation of specific, perhaps tissue or cell-type-specific F-actin structures obviously had to be dismissed as too simple. Theoretically, the required functional diversity in actin filament formation despite a limited set of powerful effectors could be achieved by combinatory mechanisms specific for a given cell biological process. However, experimental evidence for such combinatory actions of actin nucleators still is very sparse. On top of that, which mechanisms may orchestrate these powerful effectors to bring about a certain cellular processes also remains a fundamental question in cell biology.

Neurons need to extend elaborate cellular protrusions - the single signal-sending axon and multiple signal-receiving, highly branched dendrites - to form neuronal networks. These very demanding and specialized cellular morphogenesis processes are driven by the actin cytoskeleton (Kessels et al., 2011). The formation of the dendritic arbor involves local Ca^{2+} and calmodulin (CaM) signals coinciding with transient F-actin formation by the evolutionary young actin nucleator Cobl (Cordon-bleu) (Ahuja et al., 2007) at dendritic branch induction sites (Hou et al., 2015). Ca^{2+}/CaM regulates both Cobl's loading with monomeric actin and its different modes of plasma membrane association (Hou et al., 2015). Cobl is furthermore regulated via arginine methylation by PRMT2 (Hou et al., 2018). All of these aspects were required for Cobl's crucial role in dendritic arbor formation (Ahuja et al., 2007; Haag et al., 2012; Hou et al., 2015, Hou et al., 2018).

Interestingly, also Cobl's evolutionary distant ancestor Cobl-like (COBLL1; Coblr1) was recently discovered to be important for Ca^{2+}/CaM-controlled neuromorphogenesis (Izadi et al., 2018). While Cobl uses three Wiskott-Aldrich syndrome protein Homology 2 (WH2) domains to nucleate actin

3

56   (Ahuja et al., 2007), Cobl-like employs a unique combinatory mechanism of G-actin binding by its

57   single, C-terminal WH2 domain and Ca^{2+}/CaM-promoted association with the actin-binding protein

58   Abp1 (Kessels et al., 2000) to promote F-actin formation (Izadi et al., 2018). Cobl-like was also

59   found to interact with Cyclin-dependent kinase 1 and to shape prostate cancer cells by not yet fully

60   clear mechanisms (Takayama et al., 2018).

61   Here we show that Cobl and Cobl-like work at the same nascent dendritic branch sites in a strictly

62   interdependent manner choreographed by physically bridging by the membrane-binding F-BAR

63   protein syndapin I (Qualmann et al., 1999; Itoh et al., 2005; Dharmalingam et al., 2009; Schwintzer et

64   al., 2011), which we identified to interact with Cobl-like and to specifically occur in nanoclusters at

65   the convex membrane surfaces at the base of nascent membrane protrusions of developing neurons.

66   The finding that one of the three syndapin binding sites of Cobl-like was regulated by Ca^{2+}/CaM

67   unveiled a further important mechanism of local control and coordination of actin dynamics in

68   neuromorphogenesis.

69   Our work thereby provides insights into how two actin filament formation-promoting components -

70   each critical for dendritic arbor formation - power actin-mediated dendritic branch initiation in a

71   strictly coordinated manner and how this process can be directly linked to local membrane shaping to

72   give rise to the complex morphologies required for proper neuronal network formation.

73

4

74　**Results**

75　**Cobl-like and the actin nucleator Cobl work at the same dendritic branching sites and largely**

76　**phenocopy each other in their critical role in dendritic arborization**

77　The actin nucleator Cobl and its evolutionary ancestor protein Cobl-like are molecularly quite distinct

78　(**Figure 1–figure supplement 1**), however, both critical for dendritic arbor formation (Ahuja et al.,

79　2007; Izadi et al., 2018). Side-by-side loss-of-function analysis of both factors in developing primary

80　hippocampal neurons using IMARIS software-based evaluations for detailed analyses of the elaborate

81　morphology of such cells (Izadi et al., 2018) revealed surprisingly similar phenotypes (**Figure 1A-G**).

82　Dendritic branch and terminal point numbers as well as total dendritic length all were severely

83　affected by lack of Cobl-like (**Figure 1A-G**). Corresponding Cobl loss-of-function showed that,

84　while dendritic growth processes seemed largely unaffected by Cobl deficiency, also Cobl deficiency

85　led to a significant reduction of terminal points and in particular to severe loss of dendritic branch

86　points. With -35%, these defects were about as strong as those caused by Cobl-like RNAi (**Figure**

87　**1D-F**). Cobl RNAi mostly affected Sholl intersections in proximal areas. Cobl-like RNAi led to

88　reduced Sholl intersections throughout the dendritic arbor (**Figure 1G**).

89　The phenotypical comparison of Cobl and Cobl-like unveiled that both cytoskeletal effectors have

90　somewhat similar functions in dendritic arborization. Colocalization studies showed that Flag-

91　mCherry-Cobl and GFP-Cobl-like did not show any obvious spatial segregation (neither in proximal

92　nor in peripheral dendritic arbor of developing neurons) but largely colocalized. Dendritic

93　accumulations of Cobl usually showed corresponding albeit less pronounced accumulations of Cobl-

94　like (**Figure 1H,I**; arrows). This suggested that Cobl and Cobl-like are not responsible for distinct

95　branching sites but work at the same sites.

96

5

97   **Cobl-like functions in dendritic arborization strictly depend on Cobl and likewise Cobl**

98   **functions depend on Cobl-like**

99   Two powerful molecular machines for actin filament formation at the same place may either reflect

100   function redundancy or parallel action to drive cellular processes effectively in response to

101   (putatively different) signaling cues or may even reflect interlinked functions. Functional redundancy

102   seemed unlikely, because both individual loss-of-function phenotypes were severe (Cobl, -33%;

103   Cobl-like, -39%) (**Figure 1D**). Thus, we focused on the remaining hypotheses.

104   Interestingly, Cobl-like-driven dendritic arborization was completely impaired by the lack of Cobl

105   (**Figure 2A-G**). Dendritic branch point numbers, terminal point numbers and the total dendritic arbor

106   length of neurons cotransfected with GFP-Cobl-like and Cobl RNAi all were highly statistically

107   significantly below those of neurons cotransfected with Cobl-like and scrambled RNAi. The

108   suppression of the Cobl-like gain-of-function effects by Cobl RNAi was so strong that under the

109   chosen condition (34 h expression; GFP coexpression) all three parameters were indistinguishable

110   from control levels and therefore permitted the conclusion that the effects reflected a full suppression

111   of Cobl-like's functions in dendritic branching in the absence of Cobl (**Figure 2E-G**).

112   To our surprise, likewise, also Cobl-promoted dendritic arbor formation turned out to be massively

113   affected by absence of Cobl-like (**Figure 2H-K**). The dendritic parameters of developing neurons

114   expressing Cobl and Cobl-like RNAi did not show any Cobl gain-of-function phenotype but were

115   statistically not significantly different from those of control or Cobl-like RNAi (**Figure 2L-N**). Thus,

116   Cobl functions in dendritic arbor formation clearly depended on Cobl-like.

117   Taken together, Cobl and Cobl-like both are cellular factors promoting actin filament formation and

118   significantly differ in their properties, yet, in dendritic branch formation, they do not work

119   independently but surprisingly strictly depend on each other.

120

6

Cobl-like associates with syndapins

The surprising functional interdependence of Cobl and Cobl-like in dendritic arbor formation raised the question how this may be organized mechanistically with two proteins that seem to employ quite different molecular mechanisms (Ahuja et al., 2007; Izadi et al., 2018).

Using a variety of different methods, we failed to observe any obvious interactions of Cobl and Cobl-like (our unpublished efforts; also see below). Thus, the crosstalk of Cobl-like and Cobl had to be less direct and more sophisticated.

Cobl was demonstrated to use complexly choreographed membrane binding mechanisms involving its direct binding partner syndapin I (Schwintzer et al., 2011; Hou et al., 2015). Syndapins can self-associate (Kessels and Qualmann, 2006) and could therefore theoretically link Cobl and Cobl-like physically. As a prerequisite, syndapin I would have to associate with Cobl-like. Indeed, GFP-Cobl-like specifically coprecipitated with immobilized syndapin I SH3 domain. The interaction was mediated by N terminal proline-rich regions of Cobl-like (**Figure 3A**) and was conserved among syndapin I, syndapin II and syndapin III (**Figure 3B**).

In vitro reconstitutions with purified components proved that syndapin I/Cobl-like interactions were direct (**Figure 3C**) and were furthermore based on classical SH3 domain/PxxP motif interactions, as proven by using a P434L-mutated SH3 domain (**Figure 3–figure supplement 1A**).

Cobl-like deletion mutants (**Figure 3D,E**) showed that specifically three regions in Cobl-like's Cobl Homology domain (Cobl-like$^{1-111}$, Cobl-like$^{261-380}$ and Cobl-like$^{376-540}$) contained syndapin I interfaces (**Figure 3E, Figure 3–figure supplement 1B**). Each of them has a single "KRAP" motif (**Figure 1–figure supplement 1**).

Specific coimmunoprecipitation of GFP-Cobl-like$^{1-741}$ with Flag-tagged syndapin I demonstrated that the identified interaction can also occur *in vivo* (**Figure 3F**). GFP-Cobl-like$^{1-741}$ also specifically coimmunoprecipitated with Flag-syndapin II-s and Flag-syndapin III (**Figure 3–figure supplement**

7

145   **1C,D**), i.e. with syndapin family members showing a wider expression than syndapin I (Kessels and

146   Qualmann, 2004).

147   It was furthermore possible to directly visualize Cobl-like/syndapin I complex formation in intact

148   cells by demonstrating specific recruitments of GFP-Cobl-like and GFP-Cobl-like[1-741] to

149   mitochondria decorated with Mito-mCherry-syndapin I (**Figure 3G,H; Figure 3–figure supplement**

150   **1E**). This firmly excluded postsolubilization artefacts, which theoretically could compromise

151   biochemical studies. Deletion of the syndapin I SH3 domain (Mito-mCherry-SdpI$^{\Delta SH3}$) disrupted

152   complex formations with both GFP-Cobl-like[1-741] (**Figure 3I**) and GFP-Cobl-like full-length (**Figure**

153   **3–figure supplement 1F**).

154   Cobl-like/syndapin interactions also are of relevance in the brain, as immobilized, recombinant

155   TrxHis-tagged Cobl-like specifically precipitated endogenous syndapin I from mouse brain lysates

156   (**Figure 3J**). Furthermore, endogenous Cobl-like/syndapin I complexes *in vivo* were demonstrated by

157   coimmunoprecipitation analyses from mouse brain lysates (**Figure 3K**).

158

159   **Syndapin I is crucial for Cobl-like's ability to promote dendritic arbor extension and branching**

160   We next addressed whether the identified Cobl-like interaction partner syndapin I would indeed be

161   critical for Cobl-like's functions. GFP-Cobl-like massively promoted dendritic arborization already

162   after very short times (Izadi et al., 2018). Strikingly, all Cobl-like gain-of-function phenotypes in

163   developing primary hippocampal neurons were completely suppressed upon syndapin I RNAi

164   (**Figure 4C**). Cobl-like-overexpressing neurons cotransfected with syndapin I RNAi showed

165   dendritic branch points, dendritic terminal points and an overall length of the dendritic arbor that

166   were highly statistically significantly different from Cobl-like overexpression neurons and indistin-

167   guishable from those of control cells. The syndapin I RNAi-mediated suppression of Cobl-like

168   functions occurred in all dendritic arbor parts affected by Cobl-like gain-of-function (**Figure 4D-G**).

169   Cobl-like's functions in dendritic arbor formation thus are fully dependent on the availability of its

170   direct interaction partner syndapin I.

171

172   **Syndapins physically interconnect Cobl-like with Cobl**

173   In order to unravel molecular mechanisms underlying the strict functional interdependence of Cobl

174   and Cobl-like in dendritic arborization, we asked whether syndapin I may indeed be able to directly

175   bridge the two actin cytoskeletal effectors. To exclude putative indirect interactions via actin, we used

176   immobilized GST-Cobl-like[1-411], which comprises the syndapin binding sites (**Figure 3**). Cobl-like[1-

177   411] indeed formed specific protein complexes with GFP-Cobl[1-713] when syndapin I was present

178   (**Figure 5A**). No GFP-Cobl[1-713] was precipitated when syndapin I was omitted. Thus, direct

179   interactions between Cobl-like and Cobl did not occur but complex formation required syndapin I

180   acting as a bridge (**Figure 5A**). Likewise, also syndapin III mediated complex formation of Cobl-like

181   with Cobl (**Figure 5B**).

182   Demonstrating that complexes of all three components are also formed at membranes and in intact

183   cells Mito-GFP-Cobl[1-713] successfully recruiting syndapin I to mitochondrial membranes (**Figure 5–**

184   **figure supplement 1**) also recruited Cobl-like[1-741] (**Figure 5C**). The visualized complex formations

185   were specific and mediated by syndapin I acting as bridging component between Cobl and Cobl-like,

186   as omitting syndapin I did not lead to any Cobl-like[1-741] mitochondrial presence and also Mito-GFP

187   did not lead to any syndapin/Cobl-like colocalization at mitochondria (**Figure 5D,E**).

188

189   **Syndapin I and Cobl-like colocalize at sites of dendritic branch induction**

190   In line with the BAR domain hypothesis (Peter et al., 2004; Qualmann et al., 2011; Daumke et al.,

191   2014; Kessels and Qualmann, 2015; Carman and Dominguez, 2018) syndapin I may sense/induce

192   certain membrane topologies and thereby provide spatial cues for Cobl and Cobl-like functions. Thus,

193   three syndapin I-related aspects needed to be experimentally addressed: i) Where and when do Cobl-

194   like and syndapin I occur together in developing neurons? ii) Would a given syndapin I localization

195   indeed reflect specifically membrane-associated syndapin I? iii) Would putative accumulations of

196   membrane-associated syndapin I then really correspond to convex membrane topologies?

197   Dual time-lapse imaging of GFP-Cobl-like and syndapin I-mRubyRFP in developing primary

198   hippocampal neurons showed that syndapin I accumulated in defined spots along dendrites coinciding

199   with subsequent branch induction events. Such accumulations occurred as early as 1 min prior to

200   detectable dendritic branch protrusion, were spatially restricted to very small areas (diameters, ~250-

201   1200 nm) and were spatially and temporally colocalized with Cobl-like at branch initiation sites

202   (**Figure 6A,B**).

203   Afterwards, the accumulations of both proteins at the base of newly formed protrusions faded. This

204   suggested a highly mobile subpool of syndapin I and Cobl-like in the dendritic arbor.

205   Sites with repetitive dendritic protrusion attempts showed accumulations of both syndapin I and

206   Cobl-like prior to the first as well as prior to the second protrusion initiation (**Figure 6A,B**).

207

208   **Membrane-bound syndapin I occurs preferentially at protrusive membrane topologies in**

209   **developing neurons and forms nanoclusters at such sites**

210   3D-time-lapse studies do not resolve whether the observed syndapin I accumulations at nascent

211   branch sites represent membrane-associated syndapin I or a cytosolic subpool e.g. associated with

212   putative cytoskeletal components at such sites. Immunogold labeling of freeze-fractured plasma

213   membranes is a technique that *per se* exclusively focusses on membrane-integrated proteins, provides

214   membrane topology information, and can be applied to neuronal networks (e.g. see Tanaka et al.,

215   2005; Holderith et al., 2012; Schneider et al., 2014; Nakamura et al., 2015). We have recently shown

10

216 that plasma membranes of still developing neurons can in principle be freeze-fractured and

217 immunolabelled, too (Wolf et al., 2019).

218 Whereas either Cobl nor Cobl-like seemed preserved by the procedure (our unpublished data),

219 immunogold labeling of syndapin I, which can insert hydrophobic wedges into one membrane leaflet

220 (Wang et al., 2009), was successfully obtained (**Figure 7A-B**). In principle, anti-syndapin I

221 immunogold labeling was seen at both cylindrical and protrusive membrane topologies. However,

222 even at the conditions of saturated labeling applied, cylindrical membrane surfaces merely showed

223 sparse anti-syndapin I immunogold labeling and were mostly decorated with single gold particles or

224 by pairs of labels. In contrast, at protrusive sites, the labeling density was about three times as high as

225 at cylindrical surfaces (**Figure 7A,B**).

226 Protrusive sites also showed a statistically highly significant enrichment of syndapin I nanoclusters

227 ($\geq$3 anti-syndapin I labels in circular ROIs of 35 nm radius) (**Figure 7B-D)**. Interestingly, syndapin I

228 was usually not localized to the tip of the protrusion but preferentially occurred at membrane

229 topology transition zones at the protrusion base (**Figure 7A''**).

230 The accumulation of syndapin I clusters at such sites was in line with a promotion of membrane

231 curvature induction and/or with a stabilization of the complex membrane topologies found at such

232 sites by syndapin I.

233

234 **Cobl-like's N terminus is a target for the Ca^{2+} sensor CaM and Ca^{2+} signals increase Cobl-like's**

235 **associations with syndapin I**

236 The formation of neuronal networks involves local Ca^{2+} and CaM signals, which coincide with

237 transient F-actin formation at sites of dendritic branch induction (Hou et al., 2015). Cobl-like was

238 identified as Ca^{2+}/CaM target. Yet, this CaM association occurred in the C terminal part of Cobl-like

239 and regulated Cobl-like's association with the F-actin-binding protein Abp1 (Izadi et al., 2018).

11

240 Interestingly, also GFP-Cobl-like$^{1-411}$ showed Ca^{2+}-dependent CaM binding, whereas middle parts,

241 such as Cobl-like$^{376-540}$ and Cobl-like$^{537-740}$, did not (**Figure 8A,B**).

242 Surprisingly, further analyses demonstrated that the central parts of the Cobl Homology domain of

243 Cobl-like, i.e. Cobl-like$^{111-262}$ and Cobl-like$^{182-272}$ also both did not show any Ca^{2+}-dependent CaM

244 binding (**Figure 8A,B**), although the central Cobl Homology domain corresponds to the CaM-binding

245 area in Cobl (Hou et al., 2015) and represents an area of at least moderately higher sequence

246 conservation between Cobl and Cobl-like (33% identity; **Figure 1–figure supplement 1**). Instead, it

247 was the most N-terminal part of Cobl-like represented by Cobl-like$^{1-111}$ and Cobl-like$^{1-58}$ that was

248 targeted by CaM (**Figure 8A,B**).

249 Coprecipitation experiments with purified recombinant proteins confirmed that Ca^{2+}/CaM and

250 syndapin I can bind Cobl-like$^{1-411}$ simultaneously (**Figure 8C**). We hypothesized that the discovered

251 Ca^{2+}/CaM binding to the Cobl-like N terminus may play a role in regulating the syndapin binding of

252 the neighbored Cobl Homology domain. Quantitative syndapin I coimmunoprecipitation experiments

253 with Cobl-like$^{1-741}$ demonstrated an improved complex formation of Cobl-like with syndapin I when

254 Ca^{2+} was added. With an increase of ~70%, syndapin I binding to Cobl-like$^{1-741}$ turned out to be

255 massively promoted by Ca^{2+} (**Figure 8D,E**).

256 Thus, the identified N terminal complex formation with syndapin I is Ca^{2+}/CaM-regulated.

257

258 **Cobl-like's N terminal CaM binding site regulating syndapin I association levels is crucial for**

259 **dendritic arbor formation**

260 The N terminal region of Cobl-like (**Figure 1–figure supplement 1**) indeed contains putative CaM

261 binding motifs. Coprecipitation analyses clearly showed that, in contrast to GFP-Cobl-like$^{1-741}$, a

262 corresponding deletion mutant (GFP-Cobl-like$^{1-741\Delta CaM\ NT}$; GFP-Cobl-like$^{1-741\Delta 11-45}$) did not show any

263 Ca^{2+}-dependent CaM binding **(Figure 9A)**.

12

264   Strikingly, a RNAi-resistant (*) Cobl-like mutant solely lacking the N terminal CaM binding site

265   (GFP-Cobl-like*$^{\Delta CaM\ NT}$) failed to rescue the Cobl-like loss-of-function phenotypes in dendritic

266   arborization (**Figure 9B,C**). Quantitative analyses unveiled that reexpression of GFP-Cobl-like*$^{\Delta CaM}$

267   ^{NT} instead of resupplying the neurons with RNAi-insensitive wild-type Cobl-like*, which rescued all

268   Cobl-like deficiency phenotypes, led to defects in dendritic branch point numbers, terminal point

269   numbers and total dendritic length. These defects were as severe as those caused by Cobl-like RNAi

270   without rescue attempt (**Figure 9E-F**).

271   Also Sholl analyses confirmed that GFP-Cobl-like*$^{\Delta CaM\ NT}$ showed a significant lack of performance

272   in all proximal and central parts of the dendritic arbor when compared to Cobl-like RNAi/GFP-Cobl-

273   like* (statistically significantly different at all Sholl intersections up to 30 μm) (**Figure 9G**).

274   The identified N terminal CaM binding site of Cobl-like regulating the syndapin I interactions thus

275   was absolutely indispensable for Cobl-like's functions in dendritic arbor formation.

276

277   **Ca^{2+}/CaM signaling exclusively promotes the syndapin I association with the first of the three**

278   **"KRAP" motifs**

279   The critical N terminal CaM binding site was adjacent to the most N terminal of the three syndapin

280   binding areas. As a prerequisite for further analyses uncovering the regulatory mechanism, we next

281   confirmed that the interactions with syndapins were indeed solely mediated by the "KRAP" motif-

282   containing regions. Both Cobl-like$^{1-741\Delta KRAP}$ and Cobl-like$^{\Delta KRAP}$ indeed were not able to interact with

283   the syndapin I SH3 domain, as shown by coprecipitation studies and by reconstitutions of complex

284   formations with syndapin I *in vivo* (**Figure 10A,B**; **Figure 10–figure supplement 1**).

285   Strikingly, quantitative coimmunoprecipitation analyses unveiled a full abolishment of the about 50%

286   increase of syndapin I interaction with the Cobl Homology domain of Cobl-like (Cobl-like$^{1-457}$) upon

287   Ca^{2+} addition when the first "KRAP" motif (KRAP1) was deleted (Cobl-like$^{1-457\Delta KRAP1}$; Cobl-like^{1-}

13

288 $^{457\Delta59-69}$) (**Figure 10C-E**). This insensitivity of Cobl-like$^{1-457\Delta KRAP1}$ to Ca^{2+}/CaM signaling revealed

289 that it was exclusively the first "KRAP" motif (aa59-69) that was regulated by Ca^{2+}/CaM signaling.

290 Side-by-side analyses of GFP-Cobl-like$^{1-457}$ and Cobl-like$^{1-457\Delta KRAP1}$ under Ca^{2+}-free control

291 conditions revealed that without Ca^{2+} Cobl-like$^{1-457}$ and the corresponding ΔKRAP1 mutant thereof

292 coimmunoprecipitated the same amount of syndapin I (**Figure 10F,G**). Thus, without Ca^{2+} and under

293 the stringency of *in vivo* conditions, as reflected by coimmunoprecipitations, "KRAP" motif 1

294 seemed not to contribute to syndapin I complex formation but awaited activation by Ca^{2+}/CaM

295 signaling.

296

297 The single Ca^{2+}/CaM-regulated syndapin I binding site of Cobl-like is crucial for Cobl-like's

298 function in dendritic arbor formation

299 In line with the importance of the identified N terminal CaM binding site, also deletion of only the

300 first, i.e. the Ca^{2+}/CaM-regulated, syndapin I binding interface was as detrimental for Cobl-like's

301 critical functions in dendritic arborization as lacking the entire N terminal part of Cobl-like all

302 together (GFP-Cobl-like*$^{\Delta1-412}$). Both GFP-Cobl-like*$^{\Delta1-412}$ and GFP-Cobl-like*$^{\Delta KRAP1}$ completely

303 failed to rescue the Cobl-like loss-of-function phenotypes in dendritic arborization (**Figure 10H-J**).

304 Instead, cotransfections with Cobl-like RNAi in both cases merely led to dendritic morphologies

305 identical to those of neurons deficient for Cobl-like. The dendritic branch points, terminal points and

306 total dendritic length all remained significantly reduced in comparison to control neurons (scrambled

307 RNAi/GFP) and did not differ from those of Cobl-like RNAi neurons (**Figure 10H-J**).

308 This complete failure to rescue any of the Cobl-like loss-of-function phenotypes in dendritic

309 arborization demonstrated that the Ca^{2+}/CaM-regulated "KRAP" motif 1 of Cobl-like is absolutely

310 critical for Cobl-like's functions in dendritic arbor formation.

14

311   Together, our analyses unveiled that the actin nucleator Cobl and its distant relative Cobl-like - each

312   of them critical for dendritic arbor formation – in fact need to cooperate with each other in a

313   syndapin-coordinated and Ca^{2+}/CaM-regulated manner to bring about the complex morphology of

314   hippocampal neurons (**Figure 11**).

315

Discussion

Development of proper dendritic arbors of neuronal cells is key for the complex brains of vertebrates, as neuronal morphologies have direct consequences for brain organization patterns, cell-cell connectivity and information processing within neuronal networks. Here we show that this fundamental process is powered by the coordinated, strictly interdependent action of two components, which both promote the formation of actin filaments at the cell cortex, the actin nucleator Cobl (Ahuja et al., 2007) and its only distant relative Cobl-like (Izadi et al., 2018).

Cobl-like is already present in bilateria and considered as an evolutionary ancestor of the actin nucleator Cobl. Yet, we did not observe any redundant or additive functions in dendritic arborization of developing neurons. Instead, Cobl and Cobl-like both enriched at the same nascent dendritic branching sites and their functions were cooperative and each crucial for dendritic branch induction. Our findings that Cobl-like interacts with the F-BAR domain protein syndapin I providing links to Cobl and that the syndapin I-binding N terminal part of Cobl-like is regulated by Ca^{2+}/CaM signaling in a positive manner unveil the mechanisms of the striking functional interdependence of Cobl and Cobl-like (**Figure 11**).

The identified syndapin/Cobl-like interactions were mediated by three "KRAP" motif-containing regions in Cobl-like and the SH3 domain of syndapin I. Cobl-like's "KRAP" motifs are highly conserved among each other and among different species (consensus, Kr+APxpP). They furthermore show similarity to those of Cobl (consensus, KrRAPpPP) (Schwintzer et al., 2011), as well as to other mapped syndapin I binding sites, such as RRQAPPPP in dynamin I (Anggono and Robinson, 2007), RKKAPPPPKR in ProSAP1/Shank2 (Schneider et al., 2014), and KKPPPAKPVIP in the glycine receptor beta subunit (del Pino et al., 2014).

Coprecipitation of endogenous syndapin I with Cobl-like from brain extracts, coimmunoprecipitations of endogenous Cobl-like and syndapin I from mouse brain lysates as well as

16

340   visual proof of complex formation in intact cells underscore the *in vivo*-relevance of the Cobl-

341   like/syndapin I interactions we identified.

342   Syndapin I/Cobl-like interactions clearly were of functional importance, as syndapin I deficiency

343   completely suppressed Cobl-like-mediated dendritic arbor formation. In line, syndapin I accumulated

344   together with Cobl-like at nascent dendritic branch sites and membrane-bound syndapin I clusters

345   were found at convex membrane curvatures at the base of protrusions in developing neurons. With

346   their topology changes in different directions, these membrane areas fit the structure of the

347   membrane-binding F-BAR domain of syndapin I, which seems unique among the BAR protein

348   superfamily (Qualmann et al., 2011) and shows overall curvature but also a strongly kinked tilde

349   shape (Wang et al., 2009).

350   We furthermore demonstrated biochemically and in intact cells that Cobl-like and Cobl can

351   physically be interconnected by syndapin I acting as a bridge. Physical interconnection of Cobl and

352   Cobl-like by syndapin I provides a plausible molecular mechanism for the striking functional

353   interdependence of Cobl and Cobl-like and is in line with syndapin I/Cobl interactions (Schwintzer et

354   al., 2011) as well as with syndapin I's F-BAR domain-mediated self-association ability (Kessels and

355   Qualmann, 2006; Shimada et al., 2007; Wang et al., 2009) (**Figure 11**). This would leave the SH3

356   domain of each syndapin I free for recruiting effector proteins, for spatially organizing them at

357   specific, curved membrane areas at nascent dendritic branch sites and for thereby coordinating their

358   functions in dendritic branch induction.

359   Importantly, we found that the interlinkage of Cobl-like and Cobl was not static. The Cobl-

360   like/syndapin I interaction was regulated by Ca^{2+} signals. This is well in line with the involvement of

361   transient, local Ca^{2+} signals in dendritic arborization of developing neurons (Rajan & Cline 1998;

362   Fink et al., 2003; Gaudilliere et al., 2004) and with membrane targeting and cytoskeletal functions of

363   Cobl also being controlled by Ca^{2+}/CaM (Hou et al., 2015). The additional Ca^{2+}/CaM regulation of

17

364   the Cobl-like/syndapin I interface would now provide another key regulatory mechanism right at the

365   interlinking bridge between Cobl and Cobl-like.

366   The regulatory mechanism is based on an N terminal stretch of amino acids of Cobl-like proteins in

367   front of the so-called Cobl Homology domain, which is absent in Cobl proteins. With "KRAP1", Ca^{2+}

368   signaling allowed for the modulation of specifically one out of three syndapin I binding sites of Cobl-

369   like (**Figure 11**).

370   Cobl-like mutants, which either solely lacked the N terminal CaM binding site or the single

371   Ca^{2+}/CaM-regulated syndapin binding "KRAP1", both failed to rescue Cobl-like loss-of-function

372   phenotypes in dendritic branching. The N terminal CaM association regulating the

373   "KRAP1"/syndapin I interaction and consistently also the "KRAP1" thus were critical for Cobl-like's

374   functions in dendritogenesis.

375

376   Our data clearly shows that dendritic arborization of developing neurons requires the Ca^{2+}/CaM- and

377   syndapin I-coordinated, joined action of Cobl and Cobl-like. In other cells and/or cellular processes,

378   Cobl and Cobl-like also seem to have their independent, individual functions, such as the critical role

379   of Cobl in F-actin formation right beneath the sensory apparatus of outer hair cells in the inner ear,

380   the loss of which correlated with defects in pericentriolar material organization, in postnatal planar

381   cell polarity refinement and in hearing (Haag et al., 2018). Further studies of *Cobl* KO mice unveiled

382   an importance of Cobl for a specialized set of filaments interconnecting structural elements in the F-

383   actin-rich terminal web of microvilli-decorated epithelial cells in the small intestine. However, there

384   were no indications of an additional Cobl-like involvement (Beer et al., 2020). Also in proteomic

385   analyses of myoblasts, which upon IGFN1 deficiency show altered G-to-F-actin ratios, only Cobl was

386   identified but not Cobl-like (Cracknell et al., 2020).

387 Likewise, apart from dendritic branching of neurons studied here, there are no hints on any Cobl roles

388 in functions that the *Cobl-like* gene has been linked to, such as diabetes and obesity (Mancina et al.,

389 2013; Sharma et al., 2017). Cobl-like was also suggested as biomarker for different cancer types

390 (Gordon et al., 2003; Gordon et al., 2009; Wang et al., 2013; Han et al., 2017; Plešingerová et al.,

391 2017; Takayama et al., 2018), to be suppressed by Epstein-Barr virus infection (Gillman et al., 2018)

392 and to be involved in B-cell development (Plešingerová et al., 2018) but there are no hints on Cobl

393 roles in any of these processes.

394 The extension of very fine and elaborately branched cellular structures over hundreds of micrometers,

395 as in dendritogenesis of neurons, certainly represents an extreme and rather special case of cellular

396 morphogenesis. It is therefore well conceivable that a joined action of both Cobl and Cobl-like is

397 required to promote actin filament formation at locally restricted sites to drive further branching. It

398 currently seems plausible that Cobl and Cobl-like's different actin filament formation mechanisms –

399 spatial rearrangement of three actin monomers by the three WH2 domains of Cobl generating actin

400 nuclei (Ahuja et al., 2007) *versus* use of the single WH2 domain of Cobl-like and the actin-binding

401 cofactor Abp1 in a structurally not fully understood trans-mechanism (Izadi et al., 2018) – and their

402 different modes of regulation by Ca^{2+} (Hou et al., 2015; Izadi et al., 2018) represent the distinct

403 functions of Cobl and Cobl-like that have to be combined to power dendritic arborization. The

404 recently identified Cobl regulation by PRMT2-mediated arginine methylation (Hou et al., 2018) may

405 potentially also provide a unique aspect that needs to be integrated into the joined, interdependent

406 function of Cobl and Cobl-like in dendritic branch induction.

407 Although to our knowledge, besides the here reported functions of Cobl, no information on functional

408 cooperations of any actin nucleators is available for any actin cytoskeletal process in neuronal

409 function or development, some initial studies on other actin nucleators also hint towards more

410 interactive roles than initially thought. The actin nucleator Spire works with formin 2 in *Drosophila*

19

411   oocytes (Quinlan et al., 2007; Pfender et al., 2011; Montaville et al., 2014). The formin mDia1 was

412   reported to synergize with the APC protein (Okada et al., 2010; Breitsprecher et al., 2012). mDia1

413   was furthermore very recently found to indirectly interact with the Arp2/3 complex functionally

414   cooperating in cortical F-actin stiffening of mitotic HeLa cells (Cao et al., 2020). Furthermore, the

415   actin nucleator JMY was found to interact with the Arp2/3 complex in *in vitro*-reconstitutions

416   (Zuchero et al., 2009; Firat-Karalar et al., 2011). However, as JMY RNAi did not cause any

417   statistically significant decline in cell migration (Zuchero et al., 2009; Firat-Karalar et al., 2011) – a

418   process firmly established to involve the Arp2/3 complex - the functional importance of a putative

419   cooperation of JMY with the Arp2/3 complex in the formation of actin filaments remains unclear.

420   While these initial observations and the in part apparently conflicting data show that we are only at

421   the very beginning of identifying and understanding any cooperative functions of actin nucleators, the

422   here studied cell biological process of dendritic branching highlights that clearly there are actin

423   filament-driven cellular processes, which require the coordinated action of not only one but at least

424   two effectors promoting the formation of F-actin. Our mechanistic and functional studies clearly

425   demonstrate that with Cobl and Cobl-like shaping neurons into their complex morphologies involves

426   regulated and physically coordinated interactions of different actin filament formation-promoting

427   factors at the base of nascent dendritic protrusion sites.

428

429

430

431 **Material and Methods**

432 **DNA constructs**

433 Plasmids encoding for GFP-Cobl-like and parts thereof were described previously (Izadi et al., 2018)

434 and generated by PCR using the EST clone UniProtID Q3UMF0 as template, respectively. GFP-

435 Cobl-like$^{111-262}$ and Cobl-like$^{1-111}$ were generated by subcloning with the help of internal restriction

436 sites. Additional Cobl-like deletion mutants were generated by combining the following forward

437 primers, aa1 fw: 5'-AATTAGATCTATGGACCGCAGCGTCCCCGATCC-3'; aa261 fw: 5'-

438 AAAGATCTGATATCAGCAGAGAG-3'; aa537 fw: 5'-AAAGATCTAAGGATCCTGATTCAGC-

439 3'; aa740 fw: 5'-GCCTCAAGAGAATTCAGG-3'; aa376 fw: 5'-

440 TTGAATTCTTAAACCATGATCGCTTC-3'; aa182 fw: 5'- TTAGATCTCCTACACCTATAATC-

441 3' with the following reverse primers, aa457 rv: 5'- AACTCGAGCCCGGGACCAAGGGAGC-3';

442 aa538 rv: 5'-TTCTCGAGTTAATCAGGATCCTTCTC-3'; aa741 rv: 5'-

443 TCCTGAATTCTCTTGAGG-3'; aa540 rv: 5'-TTCTCGAGTTAATCAGGATCCTTCTC-3'; aa411

444 rv: 5'-GCAAGCTTGGTTTTCGAAGGTGG-3'; aa272 rv: 5'-

445 AAGAATTCTCAGTTGTGTGATATTTG-3'; aa380 rv: 5'-TTGAATTCGAAGCGATCATGGTG-

446 3'.

447 Cobl-like mutants lacking the N terminal CaM binding site Cobl-like$^{\Delta CaM\ NT}$ (Δaa11-45) were

448 generated by fusing a PCR product (primers, aa1-10+46-51 fw: 5'-

449 AAAGATCTATGGACCGCAGCGTCCCGGATCCCGTACCCAAGAATCACAAATTCCTG-3'

450 and aa741 rv: 5'-TCCTGAATTCTCTTGAGG-3') with Cobl-like$^{740-1273}$ using the internal EcoRI site

451 (corresponding to aa740/741) to obtain the respective mutated full length protein.

452 Cobl-like mutants lacking only the first "KRAP" motif (Δaa59-69; ΔKRAP1) were generated by

453 fusing a DNA fragment obtained by PCR using an RNAi-resistant Cobl-like construct (Izadi et al.,

454 2018) as template and primers aa1 fw (5'-AATTAGATCTATGGACCGCAGCGTCCCCGATCC-3')

21

455   and aa58 rv (5'-TTAAGCTTGCTCTGACAAATATG-3') with a second PCR product (primer aa70

456   fw 5'-TTAAGCTTGCCGAGACGAAGGGC-3' and aa741 rev: 5'-TCCTGAATTCTCTTGAGG-3')

457   using a HindIII site. The resulting Cobl-like$^{1-741\Delta KRAP1}$ was used to either generate Cobl-like$^{1-457\Delta KRAP1}$

458   using an internal SmaI site corresponding to aa456/457 or fused to Cobl-like$^{740-1273}$ to generate the

459   respective full length Cobl-like mutant Cobl-like$^{\Delta KRAP1}$.

460   Cobl-like mutants lacking all three "KRAP" motifs were generated by PCR using primers aa70 fw 5'-

461   TTAAGCTTGCCGAGACGAAGGGC-3' and aa333 5'-TTAAGCTTTGCATCCGAGGGC-3' rv

462   and fusing the resulting PCR product with a second PCR product obtained by using primers aa413 fw

463   5'-TTAAGCTTCTGGCTCAGACTGATG-3' and aa457 rv as well as with a PCR product resulting

464   from the above described aa1 fw and aa58 rv primers to give rise to aa59-69+334-412 deletion

465   construct (Cobl-like$^{1-457\Delta KRAP}$). Using an internal SmaI restriction site, Cobl-like$^{1-457\Delta KRAP}$ was then

466   fused to the more C terminal parts of Cobl-like to give rise to either Cobl-like$^{1-741\Delta KRAP}$ or Cobl-

467   like$^{\Delta KRAP}$ mutants.

468   A Cobl-like deletion mutant lacking the N terminal Cobl Homology domain Cobl-like$^{\Delta 1-412}$ was

469   generated by fusing a PCR product (primers, aa413 fw: 5'- TTAAGCTTCTGGCTCAGACTGATG-

470   3' and aa741 rv: 5'-TCCTGAATTCTCTTGAGG-3'; with Cobl-like$^{740-1273}$ to obtain Cobl-like$^{\Delta 1-412}$.

471   Plasmids encoding for GST fusion proteins of Cobl-like$^{1-411}$ were generated by subcloning into

472   pGEX-4T-2 (GE Healthcare). A plasmid encoding for TrxHis-Cobl-like$^{1-411}$ was generated by PCR

473   and subcloning into pET-32 (Novagen) (primers, aa1 fw: 5'-

474   AATTAGATCTATGGACCGCAGCGTCCCCGATCC-3'; aa411 rv: 5'-

475   GGGTCGACGGTTTTCGAAGGTGG-3') using EcoRI and SalI sites.

476   The RNAi construct directed against mouse and rat Cobl-like coexpressing GFP (Cobl-like RNAi#1)

477   and scrambled RNAi control were described before (Izadi et al., 2018; Pinyol et al., 2007).

478   Additionally, Cobl-like RNAi and scrambled RNAi were inserted into a pRNAT vector coexpressing

22

479   farnesylated mCherry (mCherryF) (pRNAT-mCherryF; Schneider et al., 2014). Plasmids for rescue

480   attempts were built by replacing the GFP reporter by either RNAi-insensitive, GFP-Cobl-like (Cobl-

481   like RNAi/Cobl-like* and scrambled RNAi/Cobl-like*; Izadi et al., 2018), or by mutant GFP-Cobl-

482   like sequences generated based on Cobl-like*.

483   Plasmids encoding for GST-tagged SdpI full-length and SH3 domain (aa376-441), respectively, as

484   well as for a P434L-mutated SH3 (SdpI^{SH3mut}) were described previously (Qualmann et al, 1999;

485   Qualmann and Kelly, 2000). An alternative syndapin I SH3 domain (aa378-441) was as described

486   (Braun et al., 2005).

487   Plasmids encoding for Xpress-tagged syndapin I full-length, Flag-syndapin I and mitochondrially

488   targeted syndapin I (Mito-mCherry-SdpI), syndapin I ΔSH3 (Mito-mCherry-SdpI^{ΔSH3}) and mCherry

489   (Mito-mCherry) were described by Qualmann et al. (1999), Qualmann and Kelly (2000), Kessels and

490   Qualmann (2002), Braun et al. (2005) and Dharmalingam et al. (2009), respectively. Syndapin I-

491   mRubyRFP was generated by subcloning syndapin I into a derivative of pEGFP-N1 containing

492   mRubyRFP instead of GFP (Izadi et al., 2018).

493   mCherryF-coexpressing SdpI RNAi (bp297-317; for validations see Dharmalingam et al., 2009)

494   vector and the corresponding control pRNAT vector were described previously (Schneider et al.,

495   2014).

496   GST-SdpII^{SH3} (SdpII-l, aa383-488) and GST-SdpIII^{SH3} (aa366-425) were described before

497   (Qualmann and Kelly, 2000; Seemann et al., 2017). Flag-syndapin II-s was as described

498   (Dharmalingam et al., 2009). Flag-syndapin III was generated by subcloning from GST-syndapin III

499   (Braun et al., 2005) and insertion into pCMV-tag2B.

500   GFP-Cobl, Flag-mCherry-Cobl and GFP-Cobl$^{1-713}$ were described previously (Hou et al., 2015).

501   Mito-GFP-Cobl$^{1-713}$ was generated by subcloning the respective Cobl-encoding sequence into the

502   mitochondrial targeting vector.

503 RNAi constructs against rat and mouse Cobl coexpressing farnesylated mCherry were generated by

504 subcloning into pRNAT-mCherryF (Schneider et al., 2014). The control expressing scrambled RNAi

505 and mCherryF were as described (Schneider et al., 2014).

506 Correct cloning by PCR was verified by sequencing in all cases.

507

508 **Antibodies, reagents and proteins**

509 Rabbit anti-Cobl-like antibodies were raised against a combination of two GST-Cobl-like fusion

510 proteins (GST-Cobl-like$^{537-741}$ and GST-Cobl-like$^{740-1015}$) as described previously (Izadi et al., 2018).

511 The antibodies were affinity-purified according to procedures described previously (Qualmann et al.,

512 1999; Kessels et al., 2000). Anti-syndapin I and anti-syndapin III antibodies were described

513 previously (Qualmann et al., 1999; Koch et al., 2011). Anti-GST and anti-TrxHis antibodies from

514 guinea pig and rabbit were described before, too (Qualmann and Kelly, 2000; Braun et al., 2005;

515 Schwintzer et al., 2011).

516 Polyclonal rabbit anti-GFP (ab290) was from Abcam. Monoclonal mouse anti-GFP antibodies (JL-8)

517 were from Clontech (632381). Monoclonal mouse anti-Flag (M2) and anti-MAP2 (HM-2) antibodies

518 as well as polyclonal rabbit anti-Flag antibodies (F3165, F7425) were from Sigma. Anti-Xpress

519 antibodies were from Invitrogen (46-0528).

520 Secondary antibodies used included, Alexa Fluor488- and 568-labeled goat anti-guinea pig antibodies

521 (A-11073, A-11075), Alexa Fluor488- and 568-labeled donkey anti-mouse antibodies (R37114,

522 A10037), Alexa Fluor647- and 680-labeled goat anti-mouse antibodies (A-21236, A32723), Alexa

523 Fluor488-labeled donkey anti-rabbit (A-21206), Alexa Fluor568- 647- and 680-labeled goat anti-

524 rabbit antibodies (A-11036, A-21245, A-21109) (ThermoFisher Scientific) as well as DyLight800-

525 conjugated goat anti-rabbit and anti-mouse antibodies (ThermoFisher Scientific, 35571, 35521).

526 Donkey anti-guinea pig antibodies coupled to IRDye680 and IRDye800, respectively, were from LI-

24

527   COR Bioscience (925-32411 and 926-32411). Goat anti-rabbit, anti-guinea pig and anti-mouse-

528   peroxidase antibodies were from Dianova (Jackson ImmunoResearch) (711-035-152, 106-036-003,

529   115-036-003). 10 nm gold-conjugated goat anti-guinea pig antibodies (EM.GAR10) for electron

530   microscopical examinations of freeze-fractured samples were from BBI Solutions. MitoTracker Deep

531   Red 633 was from Molecular Probes.

532   Sepharose 4B-coupled CaM was from GE Healthcare. GST- and TrxHis-tagged fusion proteins were

533   purified from *E. coli* lysates using glutathione-agarose or -sepharose (Sigma; GenScript) and Talon

534   metal affinity resin (Clontech), respectively, as described previously (Schwintzer et al., 2011;

535   Qualmann & Kelly, 2000). After purification, fusion proteins were dialyzed against PBS,

536   characterized by SDS-PAGE and snap-frozen and stored at -80°C.

537   Tag-free syndapin I and III were generated by expressing both proteins in the pGEX-6P vector (GE

538   Healthcare) and cutting of the GST tag from purified proteins using PreScission protease (GE

539   Healthcare) in 150 mM NaCl, 2 mM DTT and 20 mM HEPES pH 7.4 buffer overnight at 4°C (during

540   dialysis after elution). Cleaved off GST and uncleaved GST fusion proteins were removed with

541   glutathione-sepharose.

542

543   ***In vitro*-reconstitutions of direct protein-protein interactions**

544   Direct protein/protein interactions were demonstrated by coprecipitation assays with combinations of

545   recombinant TrxHis- and GST-tagged fusion proteins purified from *E. coli* and/or immobilized CaM

546   (GE Healthcare), respectively, in 10 mM HEPES pH 7.4, 300 mM NaCl, 0.1 mM $MgCl_2$, 1% (v/v)

547   Triton X-100 supplemented with EDTA-free protease inhibitor cocktail as well as in some cases with

548   500 μM Ca^{2+} added.

549   Eluted proteins were analyzed by SDS-PAGE, transferred to PVDF membranes by either semi-dry or

550   tank blotting and then subjected to immunodetection with anti-TrxHis and anti-GST antibodies.

25

551   Primary antibodies were detected with fluorescent secondary antibodies using a Licor Odyssey

552   System.

553

554   **Culture and transfection, and immunostaining of cells**

555   Culturing of HEK293 and COS-7 cells and their transfection using TurboFect (ThermoFisher

556   Scientific) as well as their immunolabeling was essentially done as described (Kessels et al., 2001;

557   Haag et al., 2012).

558   In reconstitutions and visualizations of protein complex formations at the surfaces of mitochondria in

559   intact cells, mitochondria of COS-7 cells were stained with 0.2 µM MitoTracker Deep Red 633 in

560   medium at 37°C for 30 min and cells were subsequently fixed with 4% (w/v) paraformaldehyde

561   (PFA) for 7 min.

562

563   **Preparation of HEK293 cell lysates**

564   HEK293 cells were washed with PBS 24-48 h after transfection, harvested and subjected to

565   sonication for 10 seconds and/or lyzed by incubation in lysis buffer (10 mM HEPES pH 7.4, 0.1

566   mM $MgCl_2$, 1 mM EGTA, 1% (v/v) Triton X-100) containing 150 mM NaCl and EDTA-free

567   protease inhibitor Complete (Roche) for 20 to 30 min at 4°C (Kessels & Qualmann, 2006). Cell

568   lysates were obtained as supernatants from centrifugations at 20000xg (20 min at 4°C).

569

570   **Coprecipitation of proteins from HEK293 cell lysates**

571   Coprecipitation experiments with extracts from HEK293 cells expressing different GFP-fusion

572   proteins were essentially performed as described before (Qualmann et al., 1999; Schwintzer et al.,

573   2011). In brief, HEK293 cell lysates were incubated with purified, recombinant GST-fusion proteins

574   immobilized on glutathione-sepharose beads (GenScript) for 3 h at 4°C. The reactions were then

575 washed several times with lysis buffer containing 150 mM NaCl and EDTA-free protease inhibitor

576 Complete. Bound protein complexes were subsequently eluted with 20 mM reduced glutathione, 120

577 mM NaCl, 50 mM Tris/HCl pH 8.0 (30 min RT) or obtained by boiling the beads in 4xSDS sample

578 buffer.

579 For coprecipitations with CaM, HEK293 cell lysates were prepared in an EGTA-free lysis buffer

580 containing 150 mM NaCl, EDTA-free protease inhibitor cocktail and 200 µM calpain I inhibitor. Cell

581 lysates were supplemented with either 1 mM EGTA or 500 µM Ca^{2+} to obtain conditions without and

582 with Ca^{2+}, respectively. After incubation with 25 µl CaM-sepharose 4B (GE Healthcare) for 3 h at

583 4°C and washing, bound proteins were isolated by boiling in 4xSDS sample buffer. Lysates,

584 supernatants and eluates were analyzed by immunoblotting.

585 Triple coprecipitations, i.e. the examinations of GST-Cobl-like[1-411]/syndapin/GFP-Cobl[1-713]

586 complexes with either syndapin I or syndapin III as bridging component were essentially performed

587 as described above (lysis buffer containing 150 mM NaCl) except that the extracts from HEK293

588 cells expressing GFP-Cobl[1-713] were not only incubated with immobilized GST-Cobl-like[1-411] but also

589 with tag-free syndapin I or syndapin III for 3 h. Bound proteins were eluted with 20 mM reduced

590 glutathione, 120 mM NaCl, 50 mM Tris/HCl pH 8.0. Eluates and supernatants were separated by

591 SDS-PAGE and analyzed by anti-syndapin I/III, anti-GST and anti-GFP immunoblotting.

592

593 **Coprecipitation of endogenous syndapin I from mouse brain lysates**

594 For coprecipitation of endogenous syndapin I, brain lysates were prepared from mice sacrificed by

595 cervical dislocation. Extracts were prepared using an Ultra Turrax homogenizer (Ika Ultra Turrax

596 T5Fu; 20000 rpm, 10 s) in lysis buffer containing EDTA-free protease inhibitor Complete and

597 supplemented with 100 mM NaCl and 200 µM calpain inhibitor I. After clearing the lysates from cell

598 debris by centrifugation at 1000xg for 20 min, the supernatants were used to precipitate endogenous

27

599 syndapin I by TrxHis-Cobl-like$^{1-411}$ fusion proteins immobilized on Talon metal affinity resin. Bound

600 proteins were eluted by boiling in sample buffer, separated by SDS-PAGE and analyzed by anti-

601 syndapin I immunoblotting.

602

603 Heterologous and quantitative coimmunoprecipitation analyses

604 Heterologous coimmunoprecipitations addressing Cobl-like/syndapin I, syndapin II and syndapin III

605 interactions were done with lysates of HEK293 cells transfected with GFP-Cobl-like fusion proteins

606 and GFP, respectively, in combination with Flag-tagged syndapins. The cell lysates were incubated

607 with anti-Flag antibodies or non-immune IgGs in lysis buffer containing 100 mM NaCl and EDTA-

608 free protease inhibitor Complete for 3 h at 4°C. Antibody-associated protein complexes were isolated

609 by 2 h incubation with protein A-agarose (Santa Cruz Biotechnology) at 4°C. The

610 immunoprecipitates were washed with lysis buffer containing 100 mM NaCl, eluted from the matrix

611 by boiling in a mix of 2 M (final) urea and SDS-sample buffer and analyzed by immunoblotting.

612 Comparisons of GFP-Cobl-like$^{1-457}$ and Cobl-like$^{1-457\Delta KRAP1}$ for their ability to associate with Flag-

613 syndapin I were also done by anti-GFP immunoprecipitations from lysates of transfected HEK293

614 cells generated according to the procedure described above.

615 For quantitative evaluations of the regulation of Cobl-like/syndapin I complexes, anti-GFP

616 immunoprecipitations of GFP-Cobl-like fusion proteins were done in the presence (2 μM CaCl$_2$

617 added) and in the absence of Ca^{2+} (1 mM EGTA added), respectively.

618 The amounts of coimmunoprecipitated Flag-syndapin I were quantified based on the detection of

619 fluorescent antibody signals using a Licor Odyssey System providing a linear, quantitative read-out

620 over several orders of magnitude. Anti-syndapin I coimmunoprecipitation signals were normalized to

621 the amounts of anti-GFP signal representing the immunoprecipitated material. This ensured that

622 similar amounts of GFP-Cobl-like proteins were examined for their extent of Flag-syndapin I

28

623 coimmunoprecipitation. Both fluorescence signals were detected on the same blot using the two

624 different fluorescence channels of the Licor Odyssey System. Data were expressed as percent

625 difference from Ca^{2+}-free conditions.

626

627 **Endogenous coimmunoprecipitations from mouse brain extracts**

628 Mice were sacrificed and the brain was cut into small pieces and homogenized in 10 mM HEPES pH

629 7.5, 30 mM NaCl, 0.1 mM $MgCl_2$ and 1 mM EGTA with protease inhibitors. Afterwards, Triton X-

630 100 was added (0.2% v/v final) and the homogenates were extracted for 1 h at 4-6°C. The samples

631 were then centrifuged at 100000xg for 30 min at 4°C and the resulting supernatants (mouse brain

632 extracts) were incubated with affinity-purified rabbit anti-Cobl-like antibodies and non-immune

633 rabbit IgGs, respectively, bound to protein A agarose (preincubation at 4°C and washing with above

634 buffer and 0.2% (v/v) Triton X-100 (CoIP buffer)). After 4 h of incubation at 6°C, the proteins bound

635 to the protein A agarose were washed with ice-cold CoIP buffer, eluted with SDS sample buffer

636 (100°C, 5 min) and analyzed by immunoblotting using anti-Cobl-like and anti-syndapin I antibodies.

637

638 **Microscopy**

639 Images were recorded as z-stacks using a Zeiss AxioObserver.Z1 microscope (Zeiss) equipped with

640 an ApoTome, Plan-Apochromat 100x/1.4, 63x/1.4, 40x/1.3 and 20x/0.5 objectives and an AxioCam

641 MRm CCD camera (Zeiss).

642 Digital images were recorded by ZEN2012. Image processing was done by Adobe Photoshop.

643

644 **Spinning disk live microscopy of developing neurons**

645 Primary rat hippocampal neurons were transiently transfected using Lipofectamine 2000 at DIV6. For

646 imaging, the culture medium was replaced by 20 mM HEPES pH 7.4, 140 mM NaCl, 0.8 mM $MgCl_2$,

29

647 1.8 mM $CaCl_2$, 5 mM KCl, 5 mM D-glucose (live imaging buffer) adjusted to isoosmolarity using a

648 freezing point osmometer (Osmomat 3000; Gonotec).

649 Live imaging was conducted at 37°C 16-24 h after transfection employing an open coverslip holder,

650 which was placed into a temperature- and CO_2-controlled incubator built around a spinning disk

651 microscope based on a motorized Axio Observer (Zeiss). The microscope was equipped with a

652 spinning disk unit CSU-X1A 5000, 488 nm/100 mW OPSL laser and 561 nm/40 mW diode lasers as

653 well as with a QuantEM 512SC EMCCD camera (Zeiss).

654 Images were taken as stacks of 7-17 images at Z-intervals of 0.31 µm depending on cellular

655 morphology using a C-Apochromat objective (63x/1.20W Korr M27; Zeiss). The time intervals were

656 set to 10 s. Exposure times of 50-200 ms and 3-12% laser power were used.

657 Image processing was done using ZEN2012 and Adobe Photoshop software.

658

659 **Culturing, transfection and immunostaining of primary rat hippocampal neurons**

660 Primary rat hippocampal neuronal cultures were prepared, maintained and transfected as described

661 previously (Qualmann et al., 2004; Pinyol et al., 2007; Schwintzer et al., 2011). In brief, neurons

662 prepared from hippocampi of E18 rats were seeded at densities of about 60000/well (24-well plate)

663 and 200000/well (12-well plate), respectively. Cells were cultured in Neurobasal^{TM} medium

664 containing 2 mM L-glutamine, 1x B27 and 1 µM/ml penicillin/streptomycin. The neurons were

665 maintained at 37°C with 90% humidity and 5% CO_2.

666 Transfections were done in antibiotic-free medium using 2 µl Lipofectamine2000 and 1 µg DNA per

667 well in 24 well plates. After 4 h, the transfection medium was replaced by conditioned medium and

668 neurons were cultured further. All analyses were done with several independent neuronal

669 preparations.

30

670   Fixation was done in 4% (w/v) PFA in PBS pH 7.4 at RT for 5 min. Permeabilization and blocking

671   were done with 10% (v/v) horse serum, 5% (w/v) BSA in PBS with 0.2% (v/v) Triton X-100

672   (blocking solution). Antibody incubations were done in the same buffer without Triton X-100

673   according to Kessels et al. (2001) and Pinyol et al. (2007). In brief, neurons were incubated with

674   primary antibodies for 1 h at RT and washed three times with blocking solution. Afterwards, they

675   were incubated with secondary antibodies (1 h, RT). Finally, the coverslips were washed with

676   blocking solution, PBS and water and mounted onto coverslips using Moviol.

677

678   **Quantitative analyses of dendrites of primary hippocampal neurons**

679   For loss-of-function analyses and the corresponding rescue experiments, as well as for suppressions

680   of Cobl-like overexpression phenotypes, DIV4 hippocampal neurons were transfected with RNAi and

681   control vectors, respectively, and fixed and immunostained about 34 h later (DIV5.5). 2-6

682   independent coverslips per condition per assay and neurons of at least 2 independent neuronal

683   preparations were analyzed based on the anti-MAP2 immunostaining of transfected neurons.

684   Transfected neurons were sampled systematically on each coverslip. Morphometric measurements

685   were based on anti-MAP2 immunolabeling of transfected neurons. Using Imaris 7.6 software, the

686   number of dendritic branching points, dendritic terminal points, and dendritic filament length were

687   determined and Sholl analyses (Sholl, 1953) were conducted.

688   For each neuron, a "filament" (morphological trace) was drawn by Imaris 7.6 software using the

689   following settings: Largest diameter, cell body diameter; thinnest diameter, 0.2 μm; start seed point,

690   1.5 x of cell body diameter; disconnected points, 2 μm; minimum segment size, 10 μm.

691   Immunopositive areas that were erroneously spliced by Imaris or protrusions belonging to different

692   cells, as well as filament branch points that the software erroneously placed inside of the cell body

693   were manually removed from the filament. Parameters determined were saved as Excel files and

31

694 subjected to statistical significance calculations using GraphPad Prism5 and Prism6 software

695 (RRID:SCR_002798).

696

697 **Freeze-fracturing and immunogold labeling**

698 Hippocampal neurons were grown for 7 days on poly-D-lysine-coated sapphire disks (diameter 4

699 mm; Rudolf Brügger, Swiss Micro Technology) in 24 well plates, washed with PBS and subjected to

700 ultrarapid freezing (4000 K/s) as well as to freeze-fracturing as described for mature neurons

701 (Schneider et al, 2014).

702 Freeze-fracturing of developing neurons led to low yields of rather fragile replica of inner and outer

703 membrane leaflets, which, however, were preserved during subsequent washing, blocking and

704 incubation (Wolf et al., 2019). Replica were incubated with guinea pig anti-syndapin I antibodies

705 (1:50; overnight, 4°C) and 10 nm gold-conjugated secondary antibodies as described for mature

706 neurons (Schneider et al., 2014).

707 Controls addressing the specificity of anti-syndapin I labeling of freeze-fracture replica included

708 evaluations of labeling at the E-face (almost no labeling) and quantitative analyses of syndapin I

709 labeling densities at control surfaces not representing cellular membranes (low, unspecific

710 immunogold labeling at a density of only $0.4/\mu m^2$). Further controls including secondary antibody

711 controls and labeling of syndapin I KO material were described previously (Schneider et al., 2014).

712 Replica were collected and analyzed using transmission electron microscopy (TEM) and systematic

713 grid explorations as described (Schneider et al, 2014; Seemann et al., 2017). Images were recorded

714 digitally and processed by using Adobe Photoshop software. All analyses were done with two

715 independent neuronal preparations.

716 Membrane areas with parallel membrane orientations (cylindrical) were distinguished from protrusive

717 topologies, as established previously (Wolf et al., 2019). Anti-syndapin I immunogold labeling

32

718   densities were determined using the complete area of the respective membrane topology on each

719   image (measured by using ImageJ).

720   Anti-syndapin I cluster analyses were conducted using circular ROIs of 70 nm diameter. Density of

721   clusters at cylindrical and protrusive membranes were calculated considering ≥3 anti-syndapin I

722   labels per ROI as one cluster. Additionally, anti-syndapin I labeling being single, paired and clustered

723   in 3 to 8 labels, respectively, was analyzed as percent of total anti-syndapin labeling.

724

725   **Statistical analyses and sample-size estimation**

726   No explicit power analyses were used to compute and predefine required sample sizes. Instead, all

727   neuronal analyses were conducted by systematic sampling of transfected cells across coverslips to

728   avoid any bias. Morphometric analyses were then conducted by using IMARIS software.

729   All data were obtained from 2-5 independent neuronal preparations seeded onto several independent

730   coverslips for each condition for transfection and immunostaining. For each condition, n numbers of

731   individual neurons ranging from about 30 to 40 were aimed for to fully cover the biological variances

732   of the cells. Higher n numbers yielded from the systematic sampling were accepted, too (e.g. see the

733   control in **Figure 1E-G** (n=45) and in **Figure 2L-N** (65)). Lower n numbers were only accepted for

734   the established Cobl overexpression phenotype (n=24) and the Cobl-like-mediated suppression if it

735   (also n=24), as results were clear and sacrificing further rats for further primary neuron preparations

736   could thus be avoided (**Figure 2L-N**).

737   Outliers or strongly scattering data reflect biological variance and were thus not excluded from the

738   analyses.

739   All n numbers are reported directly in the figures of the manuscript and all are numbers of

740   independent biological samples (i.e. neurons) or biochemical assays, as additional replicates to

741 minimize measurement errors were not required because the technical errors were small in relation to

742 the biological/biochemical variances.

743 All quantitative biochemical data (**Figure 8E**, **Figure 10E** and **Figure 10G**) are provided as bar and

744 dot plot overlays to report the individual raw data and the deviations of individual data points around

745 the mean.

746 Quantitative data represent mean±SEM throughout the manuscript. Exceptions are **Figure 10G**, in

747 which data represents mean±absolute error (n=2; no difference), and **Figure 7C**, as the percent of

748 total labeling shown in **Figure 7C** per definition has no error.

749 Normal data distribution and statistical significance were tested using GraphPad Prism 5 and Prism 6

750 software (SCR_002798). The statistical tests employed are reported in the respective figure legends.

751 Dendritic arbor parameters (number of dendritic branch points, number of terminal points and total

752 dendritic length) were analyzed for statistical significance employing 1-way ANOVA and Tukey

753 post-test throughout.

754 All Sholl analyses were tested by 2-way ANOVA and Bonferroni post-test.

755 Quantitative evaluation of syndapin I coimmunoprecipitations with Cobl-like[1-741], Cobl-like[1-457] and

756 Cobl-like[1-457ΔKRAP1] were analyzed by unpaired student's t-test.

757 Anti-syndapin I immunogold labeling densities at different surfaces of freeze-fractured replica of

758 membranes of developing neurons were analyzed by 1-way ANOVA and the densities of anti-

759 syndapin I clusters were analyzed by two-tailed Student's t-test.

760 Statistical significances were marked by * $p < 0.05$, ** $p < 0.01$, *** $p < 0.001$ and **** $p < 0.0001$

761 throughout. In addition, the numbers of p values are reported directly in the figures. Note that for p

762 <0.0001 (****) no values were provided by the software Prism 6, as the p values are too small.

763

34

764

Acknowledgments

766 We thank A. Kreusch, B. Schade and K. Gluth for excellent technical support.

767 This work was supported by *DFG* grants KE685/4-2 to MMK as well as QU116/6-2 and QU116/9-1

768 to BQ.

769

770

771

772

Author contributions

774 M. Izadi, E. Seemann, Dirk Schlobinski and Lukas Schwintzer generated data. M. Izadi, E. Seemann,

775 B. Qualmann and M. Kessels evaluated data. M. Izadi, B. Qualmann and M. Kessels designed the

776 project and wrote the manuscript.

777

778

Conflict of interests

780 The authors declare no competing financial interests.

781

782

References

Ahuja R, Pinyol R, Reichenbach N, Custer L, Klingensmith J, Kessels MM, and Qualmann B (2007) Cordon-bleu is an actin nucleation factor and controls neuronal morphology. *Cell* 131:337–350

Anggono V, and Robinson PJ (2007) Syndapin I and endophilin I bind overlapping proline-rich regions of dynamin I: role in synaptic vesicle endocytosis. *J Neurochem* 102:931-943

Beer AJ, Gonzalez Delgado J, Steiniger F, Qualmann B, and Kessels MM (2020) The actin nucleator Cobl organises the terminal web of enterocytes. *Sci Rep* 10:11156

Braun A, Pinyol R, Dahlhaus R, Koch D, Fonarev P, Grant BD, Kessels MM, and Qualmann B (2005) EHD proteins associate with syndapin I and II and such interactions play a crucial role in endosomal recycling. *Mol Biol Cell* 16:3642-3658

Breitsprecher D, Jaiswal R, Bombardier JP, Gould CJ, Gelles J, and Goode BL (2012) Rocket launcher mechanism of collaborative actin assembly defined by single-molecule imaging. *Science* 336:1164-1168

Cao L, Yonis A, Vaghela M, Barriga EH, Chug P, Smith MB, Maufront J, Lavoie G, Méant A, Ferber E, Bovellan M, Alberts A, Bertin A, Mayor R, Paluch EK, Roux PP, Jégou A, Romet-Lemonne G, and Charras G (2020) SPIN90 associates with mDia1 and the Arp2/3 complex to regulate cortical actin organization. *Nat Cell Biol* 22:803-814

Carman PJ, and Dominguez R (2018) BAR domain proteins-a linkage between cellular membranes, signaling pathways, and the actin cytoskeleton. *Biophys Rev* 10:1587-1604

Chesarone MA and Goode BL (2009) Actin nucleation and elongation factors: mechanisms and interplay. *Curr Opin Cell Biol* 21:28-37

804 Cracknell T, Mannsverk S, Nichols A, Dowle A, and Blanco G (2020) Proteomic resolution of

805 IGFN1 complexes reveals a functional interaction with the actin nucleating protein COBL. *Exp Cell*

806 *Res* 395:112179

807 Daumke O, Roux A, and Haucke V (2014) BAR domain scaffolds in dynamin-mediated membrane

808 fission. Cell 156:882-892

809 Del Pino I, Koch D, Schemm R, Qualmann B, Betz H, and Paarmann I (2014) Proteomic analysis of

810 glycine receptor β subunit (GlyRβ)-interacting proteins: evidence for syndapin I regulating synaptic

811 glycine receptors. *J Biol Chem* 289:11396-11409

812 Dharmalingam E, Haeckel A, Pinyol R, Schwintzer L, Koch D, Kessels MM, and Qualmann B

813 (2009) F-BAR proteins of the syndapin family shape the plasma membrane and are crucial for

814 neuromorphogenesis. *J Neurosci* 29: 13315-13327

815 Fink CC, Bayer KU, Myers JW, Ferrell Jr JE, Schulman H, and Meyer T (2003) Selective regulation

816 of neurite extension and synapse formation by the β but not the α isoform of CaMKII. *Neuron*

817 39:283–297

818 Firat-Karalar EN, Hsiue PP, Welch MD (2011) The actin nucleation factor JMY is a negative

819 regulator of neuritogenesis. *Mol Biol Cell* 22:4563-74

820 Gaudillière B, Konishi Y, de la Iglesia N, Yao GL, and Bonni A (2004) A CaMKII-NeuroD signaling

821 pathway specifies dendritic morphogenesis. *Neuron* 41:229-241

822 Gillman ACT, Parker G, Allday MJ, and Bazot Q (2018) Epstein-Barr virus nuclear antigen 3C

823 inhibits expression of COBLL1 and the ADAM28-ADAMDEC1 locus via interaction with the

824 histone lysine demethylase KDM2B. *J Virol* 92:e01362-18

37

825 Gordon GJ, Jensen RV, Hsiao LL, Gullans SR, Blumenstock JE, Richards WG, Jaklitsch MT,

826 Sugarbaker DJ, and Bueno R (2003) Using gene expression ratios to predict outcome among patients

827 with mesothelioma. *J Natl Cancer Inst* 95:598-605

828 Gordon GJ, Dong L, Yeap BY, Richards WG, Glickman JN, Edenfield H, Mani M, Colquitt R,

829 Maulik G, Van Oss B, Sugarbaker DJ, and Bueno R (2009) Four-gene expression ratio test for

830 survival in patients undergoing surgery for mesothelioma. *J Natl Cancer Inst* 101:678-686

831 Haag N, Schwintzer L, Ahuja R, Koch N, Grimm J, Heuer H, Kessels MM, and Qualmann B (2012)

832 The actin nucleator Cobl is crucial for Purkinje cell development and works in close conjunction with

833 the F-actin binding protein Abp1. *J Neurosci* 32: 17842–17856

834 Haag N, Schüler S, Nietzsche S, Hübner CA, Strenzke N, Qualmann B, and Kessels MM (2018) The

835 actin nucleator Cobl is critical for centriolar positioning, postnatal planar cell polarity refinement, and

836 function of the cochlea. *Cell Rep* 24:2418-2431e6

837 Han SH, Kim SH, Kim HJ, Lee Y, Choi SY, Park G, Kim DH, Lee A, Kim J, Choi JM, Kim Y,

838 Myung K, Kim H, and Kim DW (2017) Cobll1 is linked to drug resistance and blastic transformation

839 in chronic myeloid leukemia. *Leukemia* 31:1532-1539

840 Holderith N, Lorincz A, Katona G, Rózsa B, Kulik A, Watanabe M, and Nusser Z (2012) Release

841 probability of hippocampal glutamatergic terminals scales with the size of the active zone. *Nat*

842 *Neurosci* 15:988-997

843 Hou W, Izadi M, Nemitz S, Haag N, Kessels MM, and Qualmann B (2015) The actin nucleator Cobl

844 is controlled by calcium and calmodulin. *PLoS Biol* 13:e1002233

38

845 Itoh T, Erdmann KS, Roux A, Habermann B, Werner H, and De Camilli P (2005) Dynamin and the
846 actin cytoskeleton cooperatively regulate plasma membrane invagination by BAR and F-BAR
847 proteins. *Dev Cell* 9:791-804

848 Izadi M, Schlobinski D, Lahr M, Schwintzer L, Qualmann B, and Kessels MM (2018) Cobl-like
849 promotes actin filament formation and dendritic branching using only a single WH2 domain. *J Cell*
850 *Biol* 217:211-230

851 Kessels MM, and Qualmann B (2004) The syndapin protein family: linking membrane trafficking
852 with the cytoskeleton. *J Cell Sci* 117:3077-3086

853 Kessels MM, and Qualmann B (2006) Syndapin oligomers interconnect the machineries for
854 endocytic vesicle formation and actin polymerization. *J Biol Chem* 281:13285-13299

855 Kessels MM, and Qualmann B (2015) Different functional modes of BAR domain proteins in
856 formation and plasticity of mammalian postsynapses. J Cell Sci 128:3177-3185

857 Kessels MM, and Qualmann B (2020) Syndapins integrate N-WASP in receptor-mediated
858 endocytosis. *EMBO J* 21:6083-6094

859 Kessels MM, Engqvist-Goldstein AEY, and Drubin DG (2000) Association of mouse actin-binding
860 protein 1 (mAbp1/SH3P7), an Src kinase target, with dynamic regions of the cortical actin
861 cytoskeleton in response to Rac1 activation. *Mol Biol Cell* 11:393-412

862 Kessels MM, Engqvist-Goldstein AEY, Drubin DG, and Qualmann B (2001) Mammalian Abp1, a
863 signal-responsive F-actin-binding protein, links the actin cytoskeleton to endocytosis via the GTPase
864 dynamin. *J Cell Biol* 153:351-366

39

865 Kessels MM, Schwintzer L, Schlobinski D, Qualmann B (2011) Controlling actin cytoskeletal

866 organization and dynamics during neuronal morphogenesis. *Eur J Cell Biol* 90:926-33

867 Koch D, Spiwoks-Becker I, Sabanov V, Sinning A, Dugladze T, and Stellmacher A (2011) Proper

868 synaptic vesicle formation and neuronal network activity critically rely on syndapin I. *EMBO J* 30:

869 4955-4969

870 Mancina RM, Burza MA, Maglio C, Pirazzi C, Sentinelli F, and Incani M (2013) The COBLL1 C

871 allele is associated with lower serum insulin levels and lower insulin resistance in overweight and

872 obese children. *Diabetes Metab Res Rev* 29:413-416

873 Montaville P, Jegou A, Pernier J, Compper C, Guichard B, Mogessie B, Schuh M, Romet-Lemonne

874 G, and Carlier MF (2014) Spire and Formin 2 synergize and antagonize in regulating actin assembly

875 in meiosis by a ping-pong mechanism. *PLoS Biol* 12:e1001795

876 Nakamura Y, Harada H, Kamasawa N, Matsui K, Rothman JS, Shigemoto R, Silver RA, DiGregorio

877 DA, and Takahashi T (2015) Nanoscale distribution of presynaptic Ca^{2+} channels and its impact on

878 vesicular release during development. *Neuron* 85:145-158

879 Okada K, Bartolini F, Deaconescu AM, Moseley JB, Dogic Z, Grigorieff N, Gundersen GG, and

880 Goode BL (2010) Adenomatous polyposis coli protein nucleates actin assembly and synergizes with

881 the formin mDia1. *J Cell Biol* 189:1087-1096

882 Peter BJ, Kent HM, Mills IG, Vallis Y, Butler PJ, Evans PR, and McMahon HT (2004) BAR

883 domains as sensors of membrane curvature: the amphiphysin BAR structure. *Science* 303:495-499

884 Pfender S, Kuznetsov V, Pleiser S, Kerkhoff E, and Schuh M (2011) Spire-type actin nucleators

885 cooperate with formin-2 to drive asymmetric oocyte division. *Curr Biol* 21:955-960

40

886   Pinyol R, Haeckel A, Ritter A, Qualmann B, and Kessels MM (2007) Regulation of N-WASP and the

887   Arp2/3 complex by Abp1 controls neuronal morphology. *PLoS One* 2:e400

888   Plesingerova H, Janovska P, Mishra A, Smyckova L, Poppova L, Libra A, Plevova K, Ovesna P,

889   Radova L, Doubek M, Pavlova S, Pospísilova S, and Bryja V (2018) Expression of COBLL1

890   encoding novel ROR1 binding partner is robust predictor of survival in chronic lymphocytic

891   leukemia. *Haematologica* 103:313-324

892   Quinlan ME, Hilgert S, Bedrossian A, Mullins RD, and Kerkhoff E (2007) Regulatory interactions

893   between two actin nucleators, Spire and Cappuccino. *J Cell Biol* 179:117-128

894   Qualmann B and Kessels MM (2009) New players in actin polymerization--WH2-domain-containing

895   actin nucleators. *Trends Cell Biol* 19:276-85

896   Qualmann B, and Kelly RB (2000) Syndapin isoforms participate in receptor-mediated endocytosis

897   and actin organization. *J Cell Biol* 148:1047-1062

898   Qualmann B, Roos J, DiGregorio PJ, and Kelly RB (1999) Syndapin I, a synaptic dynamin-binding

899   protein that associates with the neural Wiskott-Aldrich syndrome protein. *Mol Biol Cell* 10:501-513

900   Qualmann B, Boeckers TM, Jeromin M, Gundelfinger ED, and Kessels MM (2004) Linkage of the

901   actin cytoskeleton to the postsynaptic density via direct interactions of Abp1 with the ProSAP/Shank

902   family. *J Neurosci* 24:2481-2495

903   Qualmann B, Koch D, and Kessels MM (2011) Let's go bananas: revisiting the endocytic BAR code.

904   *EMBO J* 30:3501-3515

905   Rajan I, and Cline HT (1998) Glutamate receptor activity is required for normal development of

906   tectal cell dendrites in vivo. *J Neurosci* 18:7836–7846

41

907   Seemann E, Sun M, Krueger S, Tröger J, Hou W, Haag N, Schüler S, Westermann M, Huebner CA,

908   Romeike B, Kessels MM, and Qualmann B (2017) Deciphering caveolar functions by syndapin III

909   KO-mediated impairment of caveolar invagination. *Elife* 6:e29854

910   Schneider K, Seemann E, Liebmann L, Ahuja R, Koch D, Westermann M, Hübner CA, Kessels MM,

911   and Qualmann B (2014) ProSAP1 and membrane nanodomain-associated syndapin I promote

912   postsynapse formation and function. *J Cell Biol* 205:197-215

913   Schwintzer L, Koch N, Ahuja R, Grimm J, Kessels MM, and Qualmann B (2011) The functions of

914   the actin nucleator Cobl in cellular morphogenesis critically depend on syndapin I. *EMBO J* 30:3147-

915   3159

916   Sharma V, Sharma I, Sethi I, Mahajan A, Singh G, Angural A, Bhanwer AJS, Dhar MK, Singh V,

917   Rai E, and Sharma S (2017) Replication of newly identified type 2 diabetes susceptible loci in

918   Northwest Indian population. *Diabetes Res Clin Pract* 126:160-163

919   Shimada A, Niwa H, Tsujita K, Suetsugu S, Nitta K, and Hanawa-Suetsugu K (2007) Curved EFC/F-

920   BAR-domain dimers are joined end to end into a filament for membrane invagination in endocytosis.

921   *Cell* 129:761-772

922   Sholl DA (1953) Dendritic organization in the neurons of the visual and motor cortices of the cat. *J

923   Anat* 87:387-406

924   Takayama KI, Suzuki T, Fujimura T, Takahashi S, and Inoue S (2018) COBLL1 modulates cell

925   morphology and facilitates androgen receptor genomic binding in advanced prostate cancer. *Proc

926   Natl Acad Sci USA* 115:4975-4980

927 Tanaka J, Matsuzaki M, Tarusawa E, Momiyama A, Molnar E, Kasai H, and Shigemoto R (2005)

928 Number and density of AMPA receptors in single synapses in immature cerebellum. *J Neurosci*

929 25:799-807

930 Wang Q, Navarro MVAS, Peng G, Molinelli E, Goh SL, Judson BL, Rajashankar KR, and

931 Sondermann H (2009) Molecular mechanism of membrane constriction and tubulation mediated by

932 the F-BAR protein Pacsin/Syndapin. *Proc Natl Acad Sci USA* 106:12700-12705

933 Wang Z, Yan Z, Zhang B, Rao Z, Zhang Y, Liu J, Yu L, Zhao Y, Yang B, Wu T, and Gao J (2013)

934 Identification of a 5-gene signature for clinical and prognostic prediction in gastric cancer patients

935 upon microarray data. *Med Oncol* 30:678-688

936 Wolf D, Hofbrucker-MacKenzie SA, Izadi M, Seemann E, Steiniger F, Schwintzer L, Koch D,

937 Kessels MM, and Qualmann B (2019) Ankyrin repeat-containing N-Ank proteins shape cellular

938 membranes. *Nat Cell Biol* 21:1191-1205

939 Zuchero JB, Coutts AS, Quinlan ME, La Thangue NB, and Mullins RD (2009) p53-cofactor JMY is a

940 multifunctional actin nucleation factor. *Nat Cell Biol* 11:451-459

941

942

943

944

945

946

947

948

949

43

950 **Figures legends**

951

952 **Figure 1 - Cobl-like and the actin nucleator Cobl work at the same dendritic branching sites**

953 **and largely phenocopy each other in their critical role in dendritic arborization.**

954 (**A-C**) Maximum intensity projections (MIPs) of anti-MAP2 immunostained developing primary

955 hippocampal neurons transfected as indicated at DIV4 and fixed at DIV5.5. Asterisks, transfected

956 neurons. Bars, 20 μm. (**D-G**) Quantitative comparative Cobl-like and Cobl loss-of-function analyses

957 of indicated dendritic parameters. (**H, I**) MIPs of GFP-Cobl-like and Flag-mCherry-Cobl in dendrites

958 of developing hippocampal neurons (DIV6) in standard colors (**H**) and as heat map representation (**I**),

959 respectively. Arrows, examples of putative, nascent dendritic branch induction sites with

960 accumulations of both Cobl and Cobl-like. Bar, 5 μm. Data, mean±SEM. 1-way ANOVA+Tukey (**D-**

961 **F**) and 2-way ANOVA+Bonferroni (**G**).

962

963

964 **Figure 2 - Functional interdependence of Cobl-like and Cobl in dendritic arbor formation.**

965 (**A-D**) MIPs of neurons showing the suppression of the Cobl-like gain-of-function phenotype (**B**;

966 GFP-Cobl-like+Scr. RNAi) by mCherryF-reported RNAi plasmids directed against Cobl (**C**) in

967 comparison to control neurons (**A**; GFP+Scr. RNAi) and Cobl RNAi neurons (**D**; GFP+Cobl RNAi).

968 (**E-G**) Quantitative determinations of indicated dendritic arborization parameters unveiling a full

969 suppression of all Cobl-like functions in dendritic arbor formation by a lack of Cobl. (**H-N**) Related

970 images (**H-K**) and quantitative data (**L-N**) of experiments revealing a functional dependence of Cobl

971 on Cobl-like. Asterisks, transfected neurons. Bars, 10 μm. Data, mean±SEM. 1-way ANOVA+Tukey

972 (**E-G** and **L-N**).

973

44

974

Figure 3 - Cobl-like associates with syndapins.

(**A**) Coprecipitation analyses of GFP-tagged Cobl-like and deletion mutants thereof with immobilized syndapin I SH3 domain (GST-SdpI^{SH3}). (**B**) Related coprecipitation studies with the SH3 domains of syndapin I, syndapin II (SdpII^{SH3}) and syndapin III (SdpIII^{SH3}), respectively. (**C**) Reconstitution of the association of TrxHis-Cobl-like$^{1-411}$ with purified GST-syndapin I and GST-syndapin I SH3 domain but not with GST. (**D**) Scheme of Cobl-like with its domains (PRD, proline-rich domain; RD, Abp1-binding repeat domain; WH2, WH2 domain) and deletion mutants used (red, not binding syndapins; green, binding). Red in the Cobl Homology domain, "KRAP" motifs (not drawn to scale). (**E**) Coprecipitation assays with Cobl-like deletion mutants mapping Cobl-like's syndapin binding sites. (**F**) Coimmunoprecipitations unveiling a specific association of GFP-Cobl-like$^{1-741}$ with Flag-syndapin I. (**G-I**) Reconstitution and visualization of Cobl-like/syndapin I complexes in COS-7 cells using mitochondrially targeted syndapin I (**G,H**) as well as a mutant lacking the SH3 domain (Mito-mCherry-SdpI$^{\Delta SH3}$) (**I**) with GFP-Cobl-like (**G**) and GFP-Cobl-like$^{1-741}$ (**H,I**). Bars, 10 μm. (**J**) Coprecipitation of endogenous syndapin I from mouse brain lysates by TrxHis-Cobl-like$^{1-411}$. (**K**) Endogenous coimmunoprecipitation of Cobl-like and syndapin I from mouse brain lysates.

990

991

Figure 4 - Cobl-like functions in dendritic arbor formation rely on syndapin I.

(**A-C**) MIPs of DIV5.5 neurons transfected as indicated. Asterisks, transfected neurons. Bars, 20 μm. (**D-G**) Quantitative determinations of key dendritic arborization aspects promoted by Cobl-like for their dependence on syndapin I. Data, mean±SEM. 1-way ANOVA+Tukey (**D-F**) and 2-way ANOVA+Bonferroni (**G**).

997

45

998   **Figure 5 - Cobl-like is physically linked to Cobl via syndapin I acting as a bridging component.**

999   (**A,B**) Coprecipitation analyses unveiling specific and syndapin-dependent formation of complexes

1000   composed of immobilized GST-Cobl-like, syndapin I (**A**) and syndapin III (**B**), respectively, as well

1001   as GFP-Cobl[1-713]. White lines indicate omitted blot lanes. (**C-E**) Reconstitution and visualization of

1002   Cobl-like/syndapin I/Cobl protein complexes in COS-7 cells. Mito–GFP-Cobl[1-713] (**C,D**) but not

1003   Mito-GFP (**E**) recruited mCherry-Cobl-like[1-741] in the presence of Xpress-syndapin I (**C**) but not in its

1004   absence (**D**). Boxes in **C-E,** areas presented as magnified insets (**C,D**, 4fold; **E**, 3fold). Arrows,

1005   examples of colocalization of all three channels. Bars, 10 μm.

1006

1007

1008   **Figure 6 - Cobl-like and syndapin I coincide at nascent dendritic branch sites.**

1009   (**A**) MIPs of individual frames of a 3D-time-lapse recording of a dendrite segment of a DIV7 rat

1010   hippocampal neuron coexpressing GFP-Cobl-like and syndapin I (SdpI)-mRubyRFP. Arrows, GFP-

1011   Cobl-like and syndapin I enrichments prior to protrusion initiation from these dendritic sites; *, tips

1012   of growing dendritic protrusions; (*), abandoned protrusions. (**B**) Heat map representations. Bars, 2.5

1013   μm.

1014

1015

1016   **Figure 7 - Syndapin I nanoclusters are enriched at sites of dendritic protrusion.**

1017   (**A,A',A''**) TEM images of anti-syndapin I immunogold-labeled freeze-fracture replica of developing

1018   neurons (DIV7). Red lines highlight membrane topologies protruding from regular cylindrical

1019   topology. Arrowheads, abundant and clustered anti-syndapin I immunogold labeling (10 nm) at

1020   protrusive sites. Arrows, sparse and rarely clustered anti-syndapin immunogold labeling at regular,

1021   cylindrical membrane structures. Bars, 200 nm. (**B**) Quantitative evaluations of anti-syndapin I

1022   labeling densities at protrusive and cylindrical membrane topologies. (**C**) Quantitative analysis of the

1023   relative abundance of differently clustered syndapin I labels (ROIs, 35 nm radius). In total, 335

1024   (protrusive) and130 (cylindrical) labels were evaluated. (**D**) Quantitative analysis of the density of

1025   anti-syndapin I nanoclusters ($\geq$3 anti-syndapin I immunogold labels/ROI) at regular cylindrical

1026   membrane surfaces and at those with protrusive topology. Data **B,D**, mean$\pm$SEM. 1-way ANOVA

1027   (**B**); two-tailed Student's t-test (**D**).

1028

1029

1030   **Figure 8 - Ca^{2+}/CaM associates with the N terminus of Cobl-like and positively regulates Cobl-**

1031   **like's syndapin I association.**

1032   (**A**) Scheme of Cobl-like and deletion mutants used for CaM binding studies (**B**) (red, no Ca^{2+}-

1033   dependent binding; green, Ca^{2+}-dependent binding). (**B**) Coprecipitations with immobilized CaM in

1034   presence (500 µM) and absence of Ca^{2+} and different Cobl-like deletion mutants. Green arrowheads,

1035   increased CaM interactions in the presence of Ca^{2+}. White lines, lanes omitted from blots. (**C**)

1036   Coprecipitation analyses with immobilized CaM and purified TrxHis-Cobl-like$^{1-411}$ and GST-

1037   syndapin I (GST-SdpI) showing direct and simultaneous interactions of Cobl-like$^{1-411}$ with both CaM

1038   and syndapin I. (**D,E**) Quantitative coimmunoprecipitation analyses demonstrating that Ca^{2+}/CaM

1039   signaling leads to increased syndapin I coimmunoprecipitation with Cobl-like$^{1-741}$. Blue arrowhead,

1040   position of the only faintly detected GFP-Cobl-like$^{1-741}$ in the lysates (**D**). Green arrowhead, increase

1041   of coimmunoprecipitated syndapin I (**D**). (**E**) Anti-syndapin I signal per immunoprecipitated Cobl-

1042   like (expressed as change from conditions without Ca^{2+}). Data, bar/dot plot overlays with

1043   mean$\pm$SEM. Unpaired student's t-test.

1044

1045

47

Figure 9 - The N terminal CaM binding site of Cobl-like is indispensable for all critical functions of Cobl-like in dendritic arbor formation.

(**A**) Coprecipitation analyses of Cobl-like$^{1-741}$, Cobl-like$^{1-741\Delta CaM\ NT}$ (Δ11-45) and GFP with immobilized CaM in Ca^{2+} presence and absence. Arrowhead, increased CaM interaction of Cobl-like$^{1-741}$ upon Ca^{2+} (disrupted in Cobl-like$^{1-741\Delta CaM\ NT}$). (**B-C**) Functional analyses in primary hippocampal neurons unveiling that an RNAi-insensitive (*) Cobl-like mutant lacking the N terminal CaM binding site (GFP-Cobl-like*$^{\Delta CaM\ NT}$) failed to rescue the Cobl-like loss-of-function phenotypes. Red asterisks, transfected neurons (transfection, DIV4; analyses, DIV5.5). Bars, 10 µm. (**D-G**) Quantitative evaluations of indicated dendritic parameters. Data, mean±SEM. 1-way ANOVA+Tukey (**D-F**); 2-way ANOVA+Bonferroni (**G**).

Figure 10 - Ca^{2+}/CaM signaling exclusively promotes the syndapin I association with the first of the three "KRAP" motifs and this single Ca^{2+}/CaM-regulated motif is crucial for Cobl-like's functions.

(**A**) Coprecipitations with immobilized syndapin I SH3 domain (SdpI^{SH3}) and Cobl-like and ΔKRAP mutants thereof. (**B**) MIP of a MitoTracker-stained COS-7 cell transfected with Mito-mCherry-syndapin I and GFP-Cobl-like$^{\Delta KRAP}$ (colocalization of only red and blue channels, purple in merge). Bar, 10 µm. (**C-G**) Quantitative coimmunoprecipitation analyses with GFP-Cobl-like$^{1-457}$ (**C**) in comparison to a corresponding mutant solely lacking the first "KRAP" motif (GFP-Cobl-like$^{1-457\Delta KRAP1}$) in the presence and absence of Ca^{2+}, respectively (**D**). Arrowhead, increase of coimmunoprecipitated Flag-syndapin I with GFP-Cobl-like$^{1-457}$ upon Ca^{2+}. (**E**) Quantitation anti-syndapin I coimmunoprecipitation upon Ca^{2+} presence normalized to immunoprecipitated GFP-Cobl-like$^{1-457}$ and GFP-Cobl-like$^{1-457\Delta KRAP1}$, respectively (as deviation from conditions without Ca^{2+}). (**F,G**)

1070   Side-by-side comparison of syndapin I coimmunoprecipitations with GFP-Cobl-like$^{1-457}$ and GFP-

1071   Cobl-like$^{1-457\Delta KRAP1}$ (**F**) and quantitative analysis thereof (**G**). Data, mean±absolute error. White line,

1072   lanes omitted from blot. (**H-J**) Functional analyses of the importance of Cobl-like's CaM-regulated

1073   syndapin I binding site (KRAP1) by loss-of-function rescue experiments evaluating the indicated

1074   dendritic arbor parameters of developing neurons (transfection, DIV4; analysis, DIV5.5). Note that

1075   neither a Cobl-like mutant lacking the entire N terminal part (GFP-Cobl-like*$^{\Delta 1-412}$) nor GFP-Cobl-

1076   like*$^{\Delta KRAP1}$ was able to rescue Cobl-like's loss-of-function phenotypes. Data, **E**, bar/dot plot overlays

1077   with mean±SEM. Unpaired student's t-test (**E**); mean±absolute error (**G**); mean±SEM; 1-way

1078   ANOVA+Tukey (**H-J**).

1079

1080

1081   **Figure 11 - Model depicting how Cobl and Cobl-like functions in dendritic branch initiation are**

1082   **joined, coordinated and controlled.**

1083   Cobl and Cobl-like functions are not only both critical for dendritic branch formation but both factors

1084   promoting the formation of actin filaments were found to act in an interdependent manner. The

1085   underlying mechanisms of coordination and control are depicted and include physical linkage of Cobl

1086   and Cobl-like by syndapin I forming dimers and multimeric clusters at the convexly bent membrane

1087   areas at the base of nascent branch sites. The newly identified interaction of syndapin I with Cobl-like

1088   is mediated by three independent KRAP motifs (red), the most N-terminal of which (marked by white

1089   asterisk) is regulated by a newly discovered CaM association to Cobl-like's N terminus. All

1090   mechanistic aspects unveiled in this study are depicted in detail and the corresponding functional

1091   evaluations conducted are listed in brief. The WH2 domains of Cobl and Cobl-like are shown to

1092   indicate the C terminal domains of both proteins and their cytoskeletal functions.

1093

49

1094

1095

1096   **Legends of Figure Supplements**

1097   **Figure 1–figure supplement 1 - Comparison of domain structures and alignment of Cobl-like**

1098   **with the actin nucleator Cobl.**

1099   (**A**) Scheme of Cobl-like with its domains in comparison to the actin nucleator Cobl with its domains.

1100   Abbreviations: PRD, proline-rich domain (PRD next to the Cobl Homology domain is an Abp1- and

1101   PRMT2-binding site and therefore colored in light green reminiscent of the RD, i.e. the Abp1-binding

1102   repeat domain in Cobl-like); WH2, WH2 domain. **(B)** Amino acid sequence alignment of murine

1103   Cobl-like (gi:74201419) and Cobl (gi:162135965) using Clustal Omega

1104   (https://www.ebi.ac.uk/Tools/msa/clustalo/). Marked are the Cobl Homology domains of both

1105   proteins (boxed in light blue) and the "KRAP" motifs (boxed in red) of both proteins. Furthermore,

1106   the single C terminal WH2 domain of Cobl-like and the three WH2 domains of Cobl are marked by

1107   orange letters. The CaM binding region of Cobl in the Cobl Homology domain and in the C terminal

1108   CaM binding regions in Cobl and Cobl-like are boxed in yellow, the Abp1- and PRMT2-binding

1109   PRD of Cobl is boxed in light green. The Abp1-binding repeat domain of Cobl-like is boxed in green

1110   and the proline-rich region located N terminal of the Abp1-binding area is boxed in purple. Note that

1111   although Cobl-like is considered as evolutionary ancestor of Cobl, the sequence conservation

1112   between both proteins in general is very low (*, identity; ":", high similarity; ".", moderate

1113   similarity). Even in the most-conserved part, the so-called Cobl Homology domain, the similarity is

1114   limited to the central core of this proposed domain and to the "KRAP" motifs.

1115

1116

1117

1118 **Figure 3–figure supplement 1 - Cobl-like associates with syndapins.**

1119 (**A**) Immunoblot analyses of a reconstitution of the association of TrxHis-Cobl-like$^{1-411}$ with

1120 recombinant, purified GST-syndapin I and GST-syndapin I SH3 domain but not with a mutated

1121 syndapin I SH3 domain (P434L; SdpI^{SH3mut}). (**B**) Anti-GFP immunoblotting of the GST controls of

1122 the syndapin I coprecipitation assays with Cobl-like deletion mutants shown in **Figure 3E**. (**C,D**)

1123 Immunoblotting analyses of specific coimmunoprecipitations of GFP-Cobl-like$^{1-741}$ but not GFP with

1124 Flag-tagged syndapin II-s (short splice variant, SdpII-s) and syndapin III (SdpIII). (**E,F**) MIPs

1125 showing control experiments accompanying the protein complex reconstitutions between GFP-Cobl-

1126 like and GFP-Cobl-like$^{1-741}$ and mitochondrially targeted syndapin I (Mito-mCherry-SdpI) shown in

1127 **Figure 3G-I**. (**E**) GFP is not recruited to Mito-mCherry-SdpI-enriched sites. (**F**) GFP-Cobl-like is not

1128 recruited to mitochondria when a Mito-mCherry-SdpI lacking the SH3 domain (Mito-mCherry-

1129 SdpI$^{\Delta SH3}$) is coexpressed. Bars, 10 µm.

1130

1131

1132 **Figure 5–figure supplement 1 - Recruitment of syndapin I to mitochondrial surfaces in intact**

1133 **cells by Mito-GFP-Cobl$^{1-713}$.**

1134 Reconstitution and visualization of Cobl/syndapin I protein complexes inside of intact COS-7 cells.

1135 Mitochondrially targeted Cobl$^{1-713}$ (green in merge) recruits Xpress-tagged syndapin I (red in merge;

1136 anti-Xpress immunolabeling) to mitochondria (blue in merge; visualized by MitoTracker). Boxes

1137 mark the area presented as magnified inset (4fold enlargement). Colocalization of all three channels

1138 appears in whitish colors (white, beige, turquoise, rosé) in the merge. Bar, 10 µm.

1139

1140

51

1141   **Figure 10–figure supplement 1 - The three "KRAP" motifs are critical for Cobl-like's**

1142   **association with syndapin I.**

1143   (**A**) Anti-GFP immunoblotting of control experiments of the coprecipitation analyses shown in

1144   **Figure 10A** demonstrating that neither Cobl-like nor any of the Cobl-like mutants associated with

1145   GST. (**B,C**) MIPs of COS-7 cells transfected with Mito-mCherry-syndapin I and GFP-Cobl-like$^{1-741}$

1146   (**B**) and a GFP-Cobl-like mutant lacking the regions with the three "KRAP" motifs (GFP-Cobl-like^{1-}

1147 $^{741\Delta KRAP}$) (**C**), respectively. Note the successful recruitment of GFP-Cobl-like$^{1-741}$ to syndapin I-

1148   decorated mitochondria (colocalization of all three channels shown appears white in merge; examples

1149   are marked by arrowheads; **B**), whereas the corresponding GFP-Cobl-like$^{1-741\Delta KRAP}$ was not recruited

1150   to mitochondria (colocalization of only Mito-mCherry-syndapin I (red in merge) and MitoTracker

1151   (blue in merge) appears purple in merge; **C**). Bars, 10 µm.

Figure 1

Figure 1–figure supplement 1

A
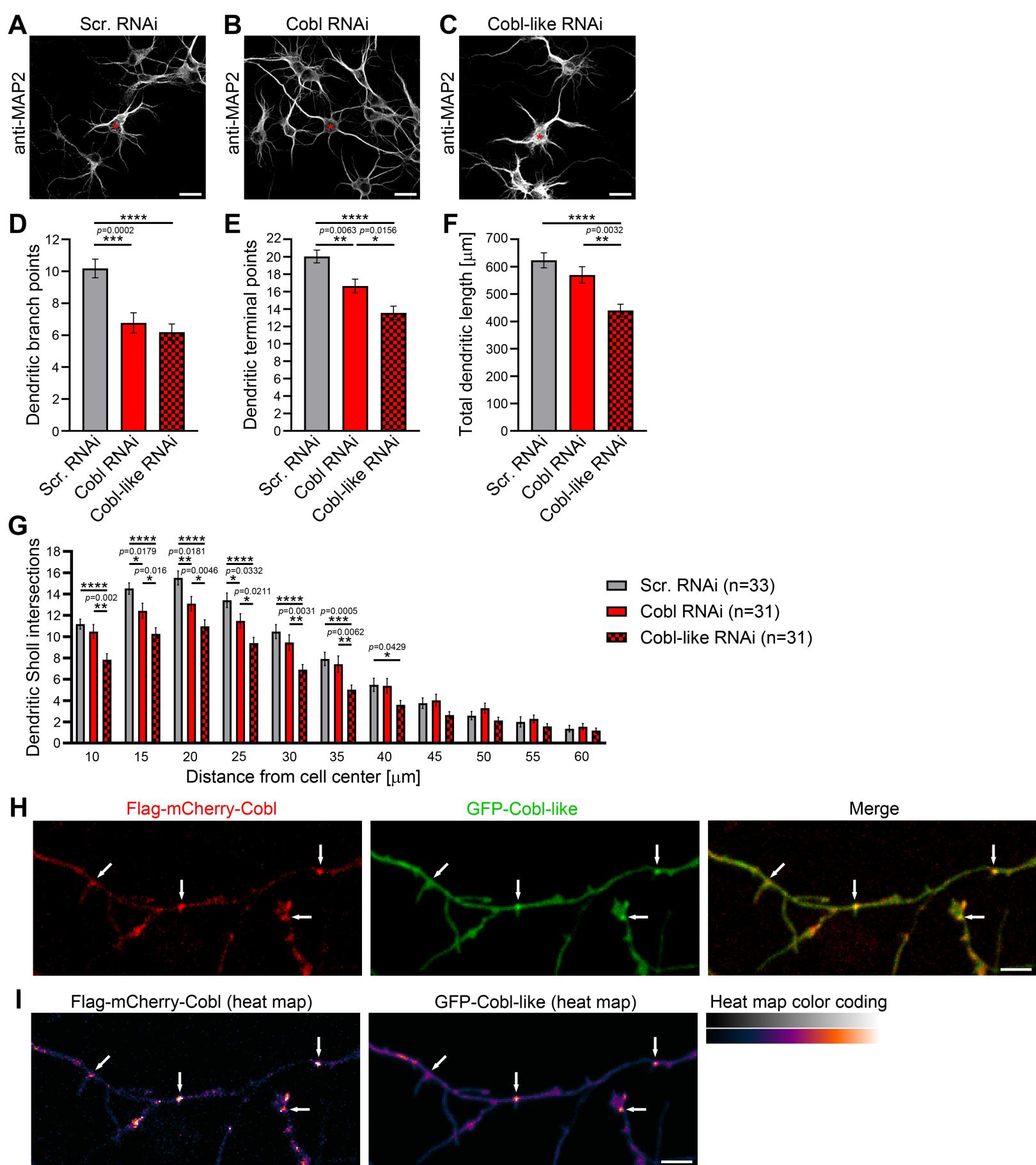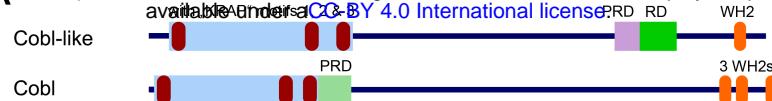
Cobl-like

Cobl

B

```
Cobl-like    MDRSVPDPVPRSAPRTPAMQPAGSAGKRRFMKMFHAHSKNDFVRIKNHKFLPLHICQSRK  60
Cobl         ----------------------------------------------MDAPRALAAKPPTGRK  16
                                                         :.  : *  :  .**

Cobl-like    TKGKAPLPPAETKGTDVSSAEDP-----VESTAVVTEQQDNMIDKDIELSVVLPGDILKS  115
Cobl         MKARAPPPPGKPAAQNVHSEQKLPHDATLGSQQSLVYMKEALQNSTLDITVVLPSGLEKQ  76
             *.:** **.:  .  :* * :.       : *   :.  :: : :. :::::****..: *.

Cobl-like    TTVHGSKPMMDLLVFLCAQYHLNPSSHTIDLLSAE-ENLIKFKPNTPIGMLDVEKVILKP  174
Cobl         SVVSGSHAMMDLLVELCLQNHLNPSHHVLEIWSSETQQPLSFKPNTLIGSLNVHTVLLKE  136
             :.* **: ****** ** * ***** *.::: *:* :: :.***** ** *:*..*:**

Cobl-like    KSLDKKK--PTPIIPEKTVRVVINFKKTQKTIVRVSPHTPLQDLAPIICSKCEFDPLHTV  232
Cobl         KVPEERVKPGLTKAPEKSVRLVVNYLRTQKAVVRVSPEVPLQNILPVICAKCEVNPEHVI  196
             *  :::    ***:**:*:*: :***:*****.***:: *:**:***.:* *.:

Cobl-like    LLKDYQAQEPLDLTKSLNDLGLRELYAMDISRESCQISHNPDIVKEKENKGIFSFFQRSK  292
Cobl         LLRDNVAGEELELSKSLNELGIKELYAWDNRREMFRKSSLGNDETDKEKKKFLGFFKANK  256
             **:*  * * *:*:****:**::**** *  **  : *   :  .:**:* ::.**: .*

Cobl-like    KKREQTASAPATPLVS------------------------KHRPSFTRSNTISKPYISNT  328
Cobl         RSNSKAEHLGLSGADSDEDPAKSASGGDLNGCVTTPNSPSLHSRSLTLGPSLSLGNISGV  316
             :...::    :  : *                    *  *:* . ::*   **..

Cobl-like    LPSDAPKKRRAPLPPMPTSQGAAQGQERRASCVERSTSVDDTDKSSSEAIMVRTGSLQLS  388
Cobl         SMKSDMKKRRAPPPPSPKLLGQDKVSEKAS-----------------------------  346
             ..  ***** ** *.  *  : .*: :

Cobl-like    STSVGTSSLKRTKRKAPAPPSK--TP---LAQT------DERNSAMAHGLPLEDGIAPDS  437
Cobl         --LSSQADLQKKKRKAPAPPPPQQPPPSPVVPNRKEDKEENRKSTVGVGRQVP-------  397
                . :.*::.**:*****      *   :. .    ::*:*::. * :

Cobl-like    MLELSSPEGMSTPEGSLGPGFLS-QEQCAVPKPPDEI-------SEGPGTPETAV---AS  486
Cobl         ---QKPPRGTA-----RGPPQLVLPPPPPYPPPDTDVTEPVTFPGEGAGSETSELRPKLS  449
                . *.* :     ** *     * * ::        .** *: : :    *

Cobl-like    LTSGVSSDYSLEEIDE-----KEELSEASKDPAGSISVKSPDIAS--ASTDMRITVEKDP  539
Cobl         LPLGPGSHCSMGGVSQVPAESEETASEDTTEDSGVMSSPSDAISLDSQQDSMRSKDKWST  509
             *  * .*.* *: :.:      :* ** :.: :* :* *  * *:     . .** . :.

Cobl-like    DSALGISDGETSPSSKGNTQEGRSTEGQGPYHP-VVCHIGNEDRVSDSIKDMKTLGPNQE  598
Cobl         DQ-----------EDGSDQDLAGTPELGPQKSPSWGKSGSGSSI---LRTEKATMPTND  554
             *.            ..*. *: .*   ** :    : *. . :   :: *:  *.::

Cobl-like    SVVQNEIMVCATSTDYVKNRPGKMETTIEGEGEALKKASDMETDRLSGS-----------  647
Cobl         ---DEDLFITGH----LHQTLAELDEDLEGMEENYETDTSSLTNSVNGVSNHSLQEAIIP  607
                :::::: .     ::: .::: :**  *  :. :.  *: :.*

Cobl-like    -------------------------PACRM------DSVKSSRENHLTAS---------  666
Cobl         DSGVDDIPVTFIGEVSDEPFDSGLFSSRCNNATTFNTGSIAS-QRSHLSPSQTEHSQPFV  666
                                      *.        .*: * :..**: *

Cobl-like    --------PGP----DQKLNQPGVEKTKMQDAAIQATPARDTFDGNHEVSNSSDPRADET  714
Cobl         RTSRKEPDPSPPSQDNRKRNQPTLANTSENENPVETD-----------------P----T  705
                     *.*     ::* *** : :*. :: :::                    *    *

Cobl-like    VQTSDGSISAQHSSANVQDSVNASREFRSQGTSTYVQDRLPEKEPACTYGNNVPLSPVDG  774
Cobl         VT-------SLVSKLLIDD-PKAKDKGKVHGSS------HSEKTQAGHGINSLRVNPRDG  751
             *         :  *.  ::*  :*.  : :  :*:*          ** *     *.: :.* **

Cobl-like    SNKNPAASYLKNFPLYRQDSNPKPKPSNEITREYIPKIGMTTYKIVPPKSLEMVKDWESE  834
Cobl         KDESSN----------SAPPPWSHHGQALGGSYGLKYGLTTYKIVPPKSEMRCYDRDVS  800
             .::.               .   * : .: :  .*  * *:*********      * : .

Cobl-like    AVGRKDDQKMLPVGQKHTIENMTETSMQTEVPATSKSSQQPQPDLKPKPSSGTERHLH--  892
Cobl         LST--GAIKIDELG------NLVSPHMNGSRTISP-PSAVVET---DTPPIGKVKEFWRR  848
              . *: :*       *:.. *: .   :  *  :      .*  *. :.:

Cobl-like    ----RTLSSPT---------GTETNPPKPPPRVTT-------------DTGTIPFAPNLED  926
Cobl         NSMEKYLNGPAECTIKRAPSTTITATPEKPQQDNGMKAAFTVTTPQQQPASQEYGAHLEE  908
                 : *..*:          * *  *: *: .    **    :     : .: :. :**:

Cobl-like    INNILESKFRSRASNPQAK-PSSFFLQMQKRASGHYVTSAAAKSVHTAPGPA----PKEP  981
Cobl         ERSRPQSAVSCSVKVPASNPTDITFLKPQRRTSSQYVASAIAKKMGPPKVHADVVRPHKA  968
             ..  :*  .  . .*  * :: .  **: *:*:*.:**:** **.:       *     *:

Cobl-like    TIKEVQ--------------RDPQLSPEQRPSSLSERTHSAPLPNISKADDDIIQKPAE  1026
Cobl         TTEQCHEEAKLARSPPTRKDDAAPNLHSEARQHEHGTNQSSVCLPS-----NPGVQLPAG  1023
             * :: :              *:*  * *  . . . *. **.      :  :* **

Cobl-like    TS----------------PPPVAPKPMTLPAET-------------------------  1043
Cobl         GHPKVEVNSTYGKSSTQDYPAAVHRNSYFLPGRSSHRDRVSVGQSCGFNEKQTTSNQKAN  1083
                            *  *  :   **..:

Cobl-like    ------------SPPPVAAK-----------PVALPAETSPPPVAPKPMTLPAETSLPPV  1080
Cobl         STSNFSQALDKAHPPPLLLAEARDSGRILMNGSARTPGNCEPPHSPKESTLTS-------  1136
                        ***:               *     .. ** :** ** :

Cobl-like    FPKPMTLRAETSPPPVAAKPVALPGSQGTSLNLKTLKTFGAPRPYSSSGPSPFALAVVKR  1140
Cobl         ---YIILQTEEKPSSLST-----DGQ--DADDTLPSSIFGPKKKFKPVIQRPLPKDVSLH  1186
                : *::* .* ::        *.  : :    . ** : :.     *:   *  :

Cobl-like    SQSF----------SKACPESASEGSSALPPAATQD-------------------  1166
Cobl         SLASEELQSFRNAALGAPG--LD---KPQQEDLGLPPPPALPPPPAPAQQAPSASVTVSR  1246
             *  :          :     *  *.:.**    *   .:

Cobl-like    ----EKTHTVNKPMVGSQHGDVDKQNNPVQNEH---SSQVLTPAD-----GPSFTLKRQS  1214
Cobl         SLASEELQSFRNAALGAPG--LD---KPQQEDLGLPPPPALPPPPAPAQQAPSASVTVSR  1301
                 *: ::..:  :*:     :*    :* *::          .* *         .** ::.  .

Cobl-like    SLTFQSSDPEHVRQSLLTAIRSGEAAAKLKRVTVPSNTISVNGKSGLSQSMSIDAQDSR  1273
Cobl         FSTGTPSNSVNARQALMDAIRSGTGAARLRKVPLLV-----------------------  1337
                 *    *: :.**:*: ***** .**:*::* :
```

Figure 2

Figure 3

Figure 3-figure supplement 1
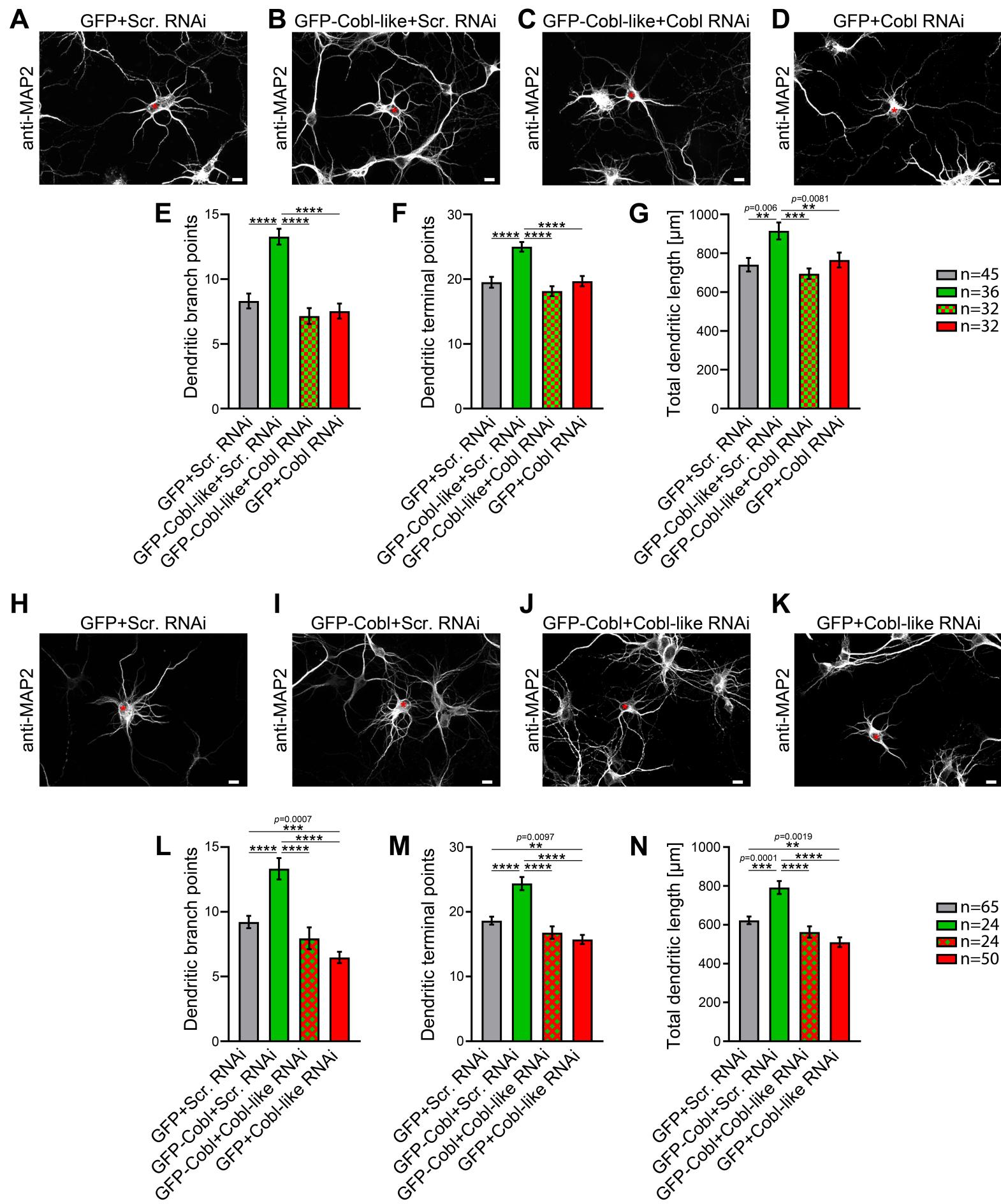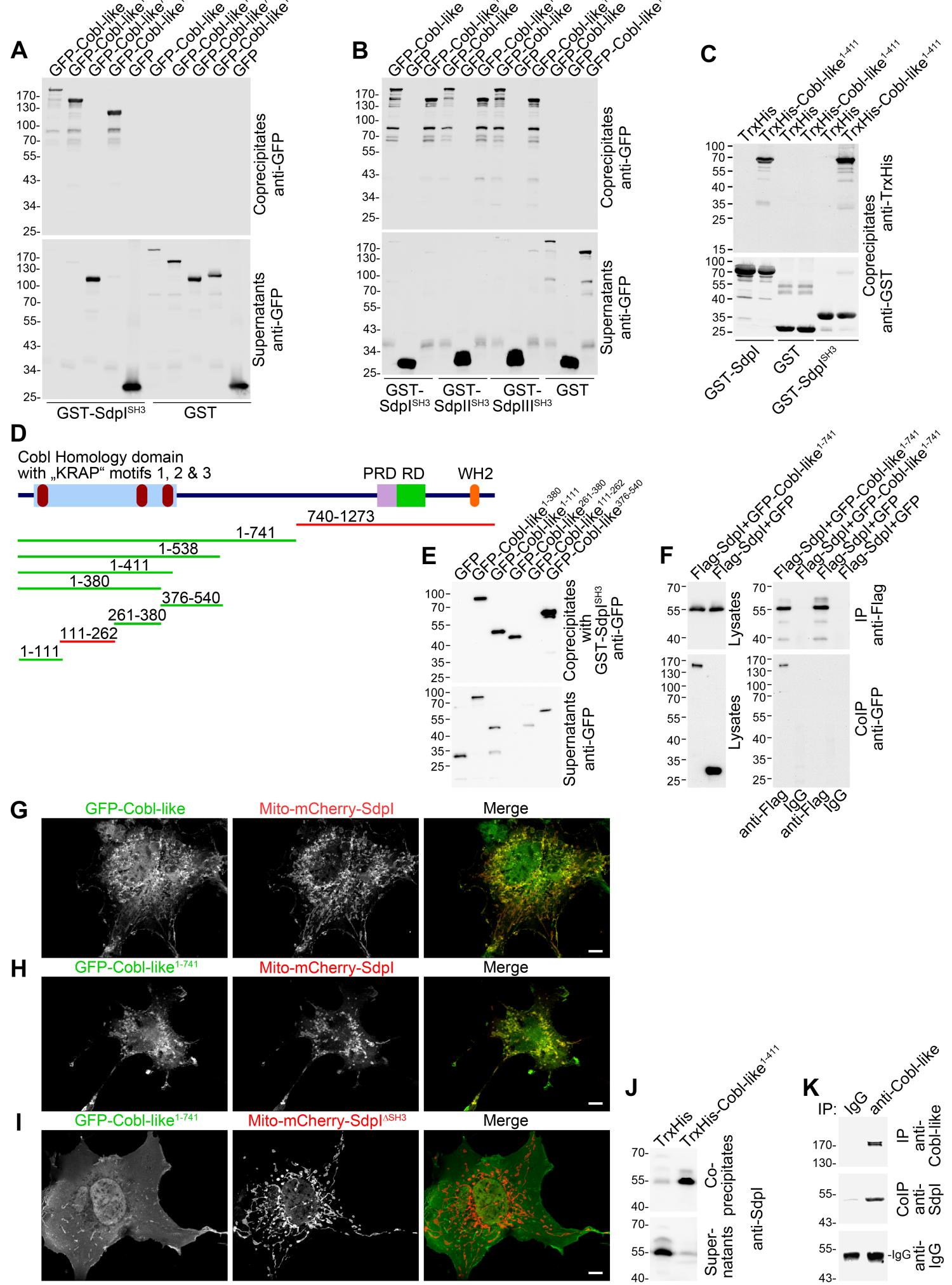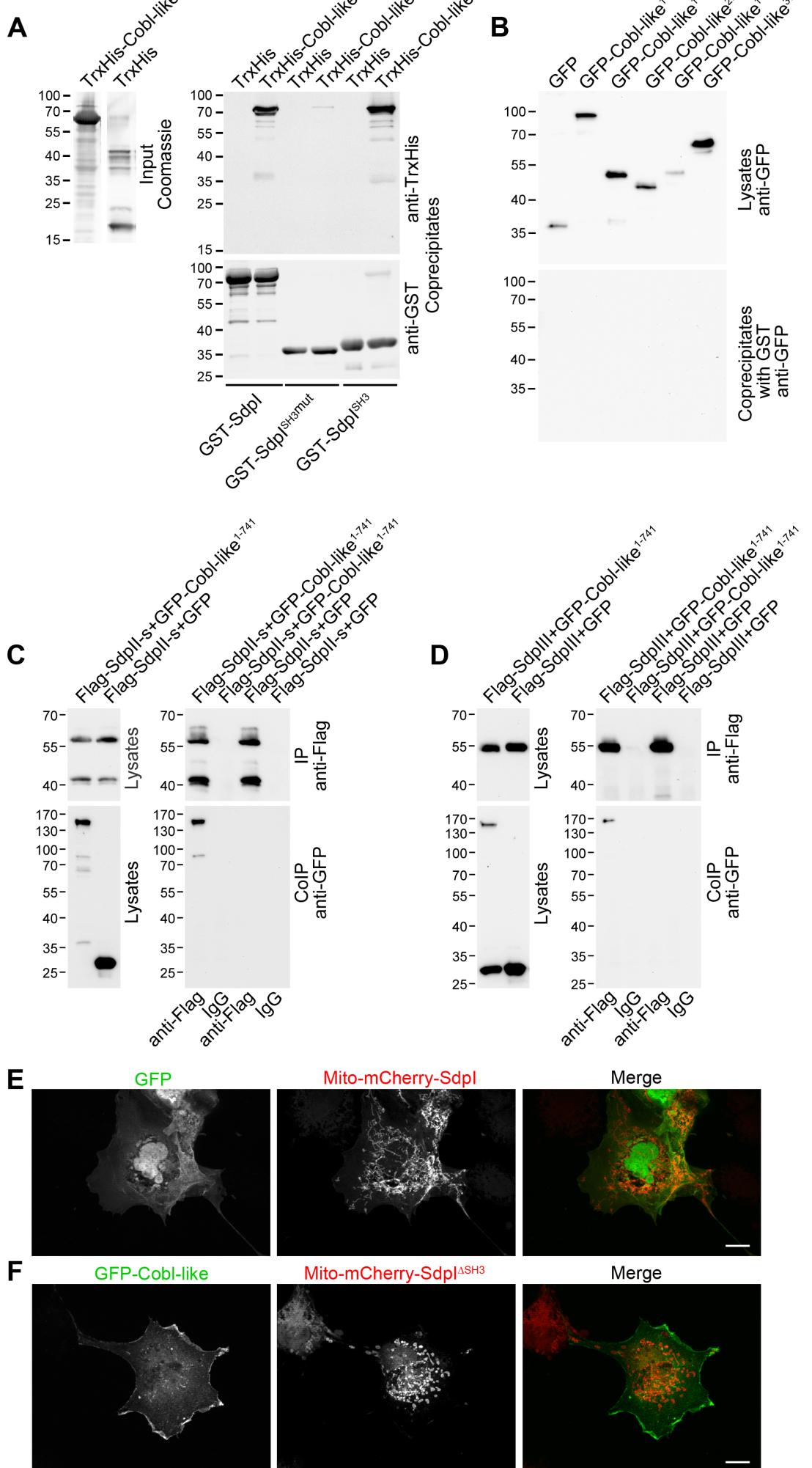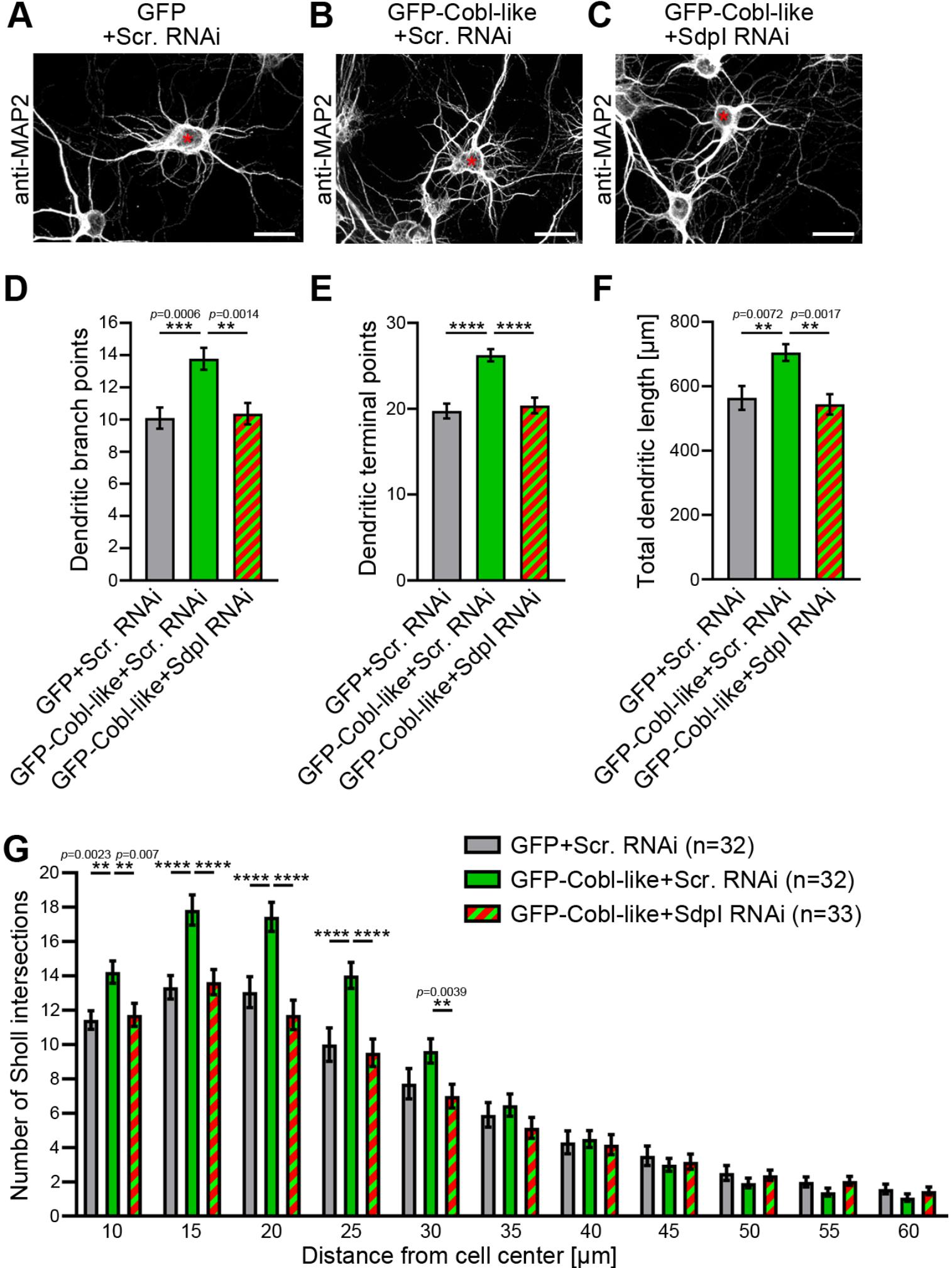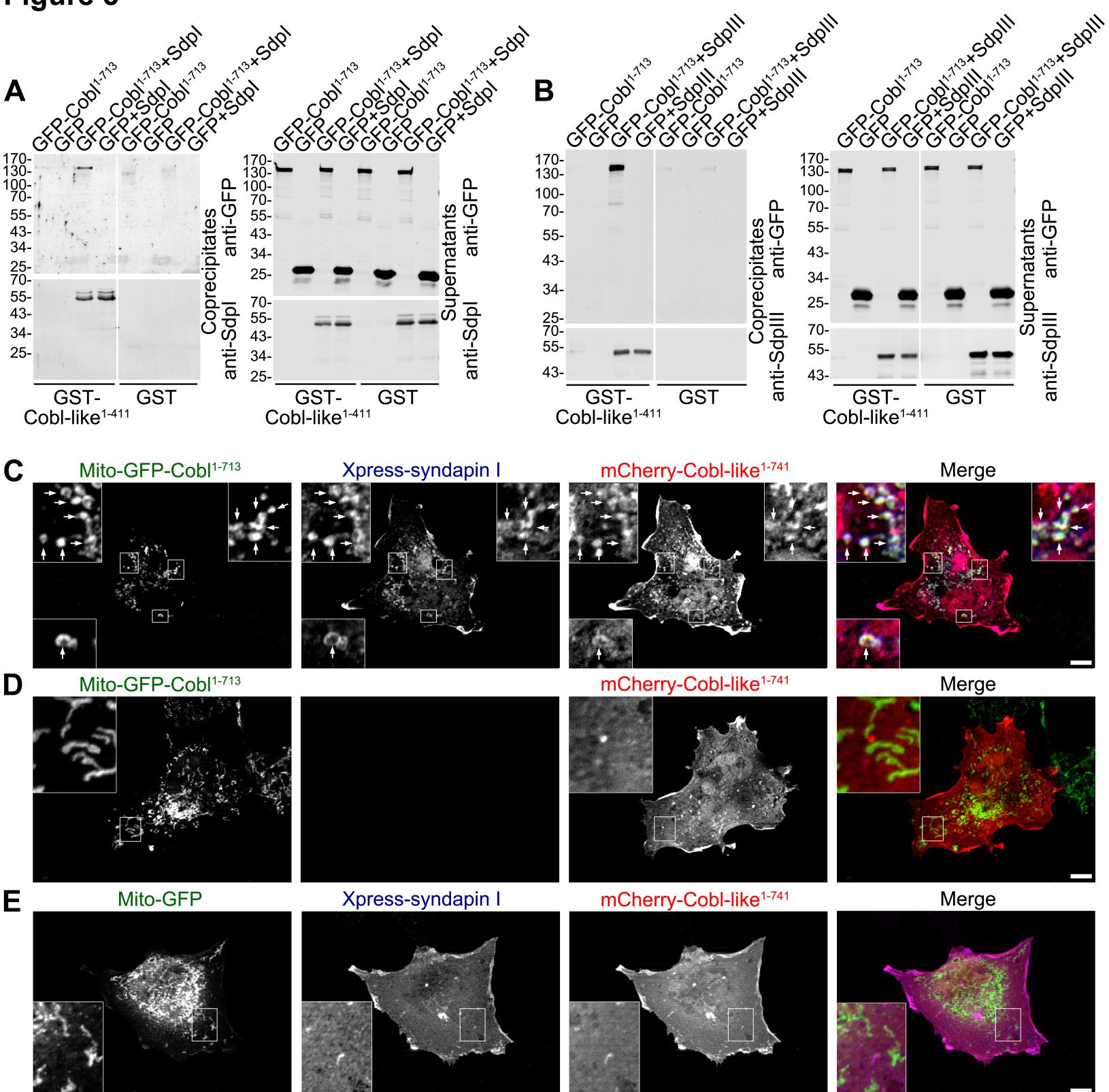
Figure 4

Figure 5

# Figure 5–figure supplement 1
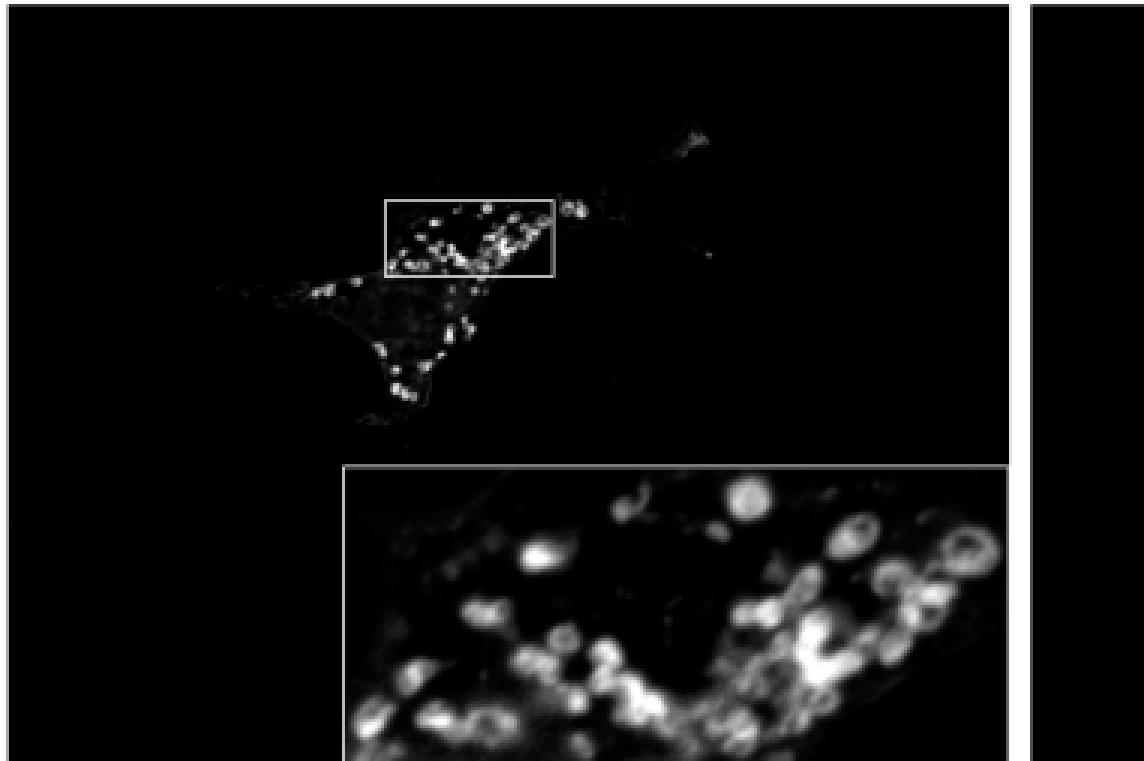
| Mito-GFP-Cobl$^{1-713}$ | Xpress-syndapin I | MitoTracker | Merge |
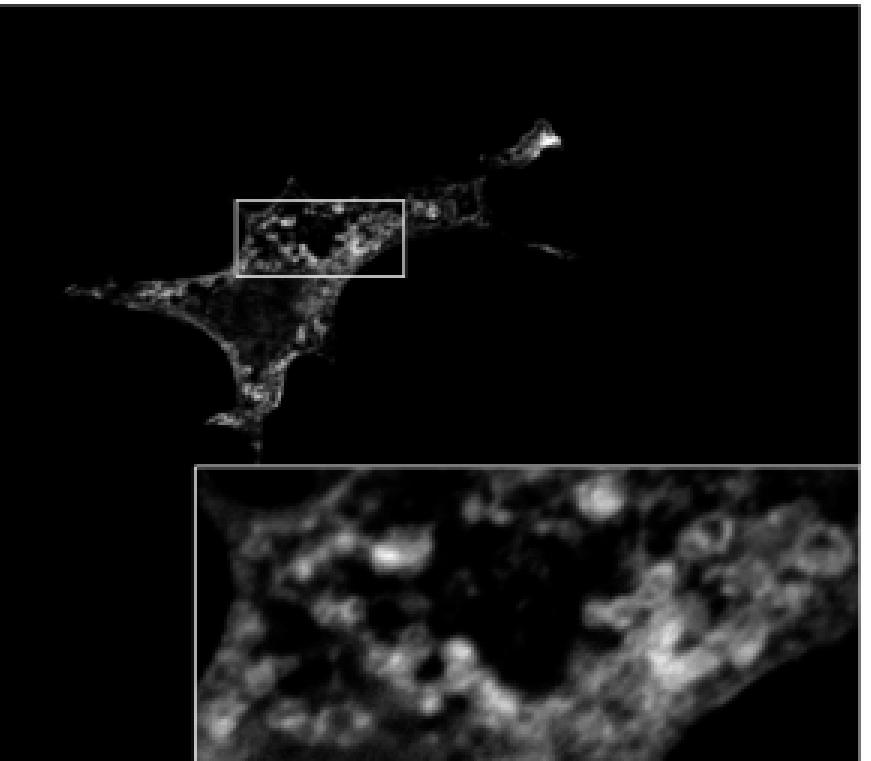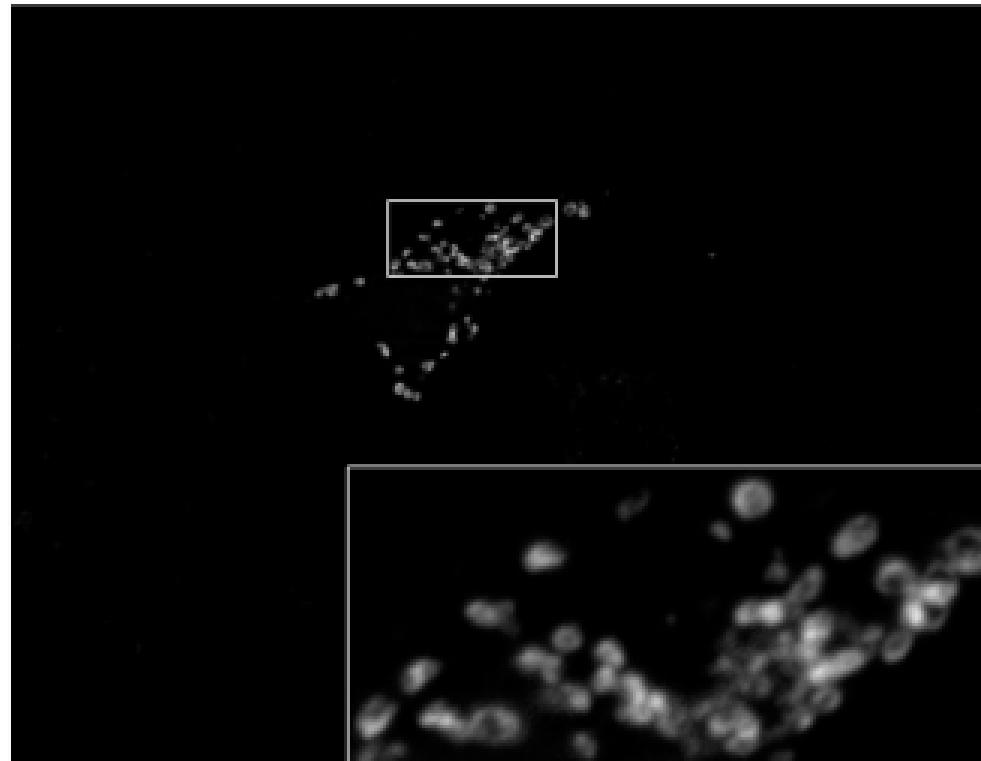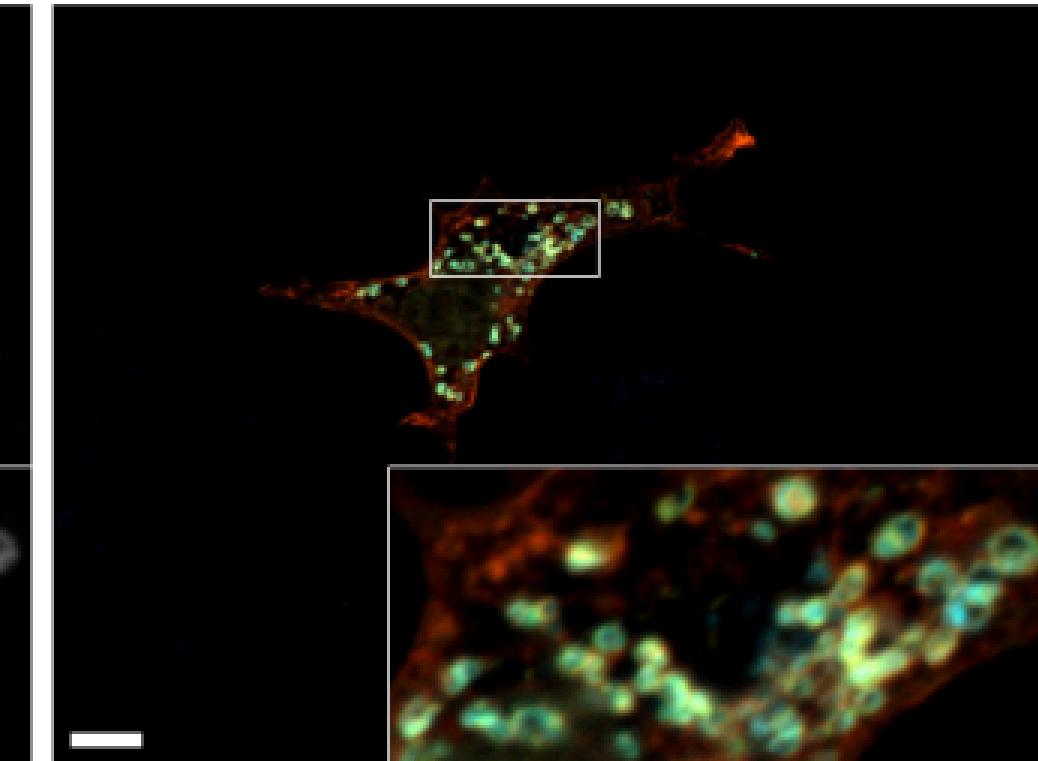
Figure 6
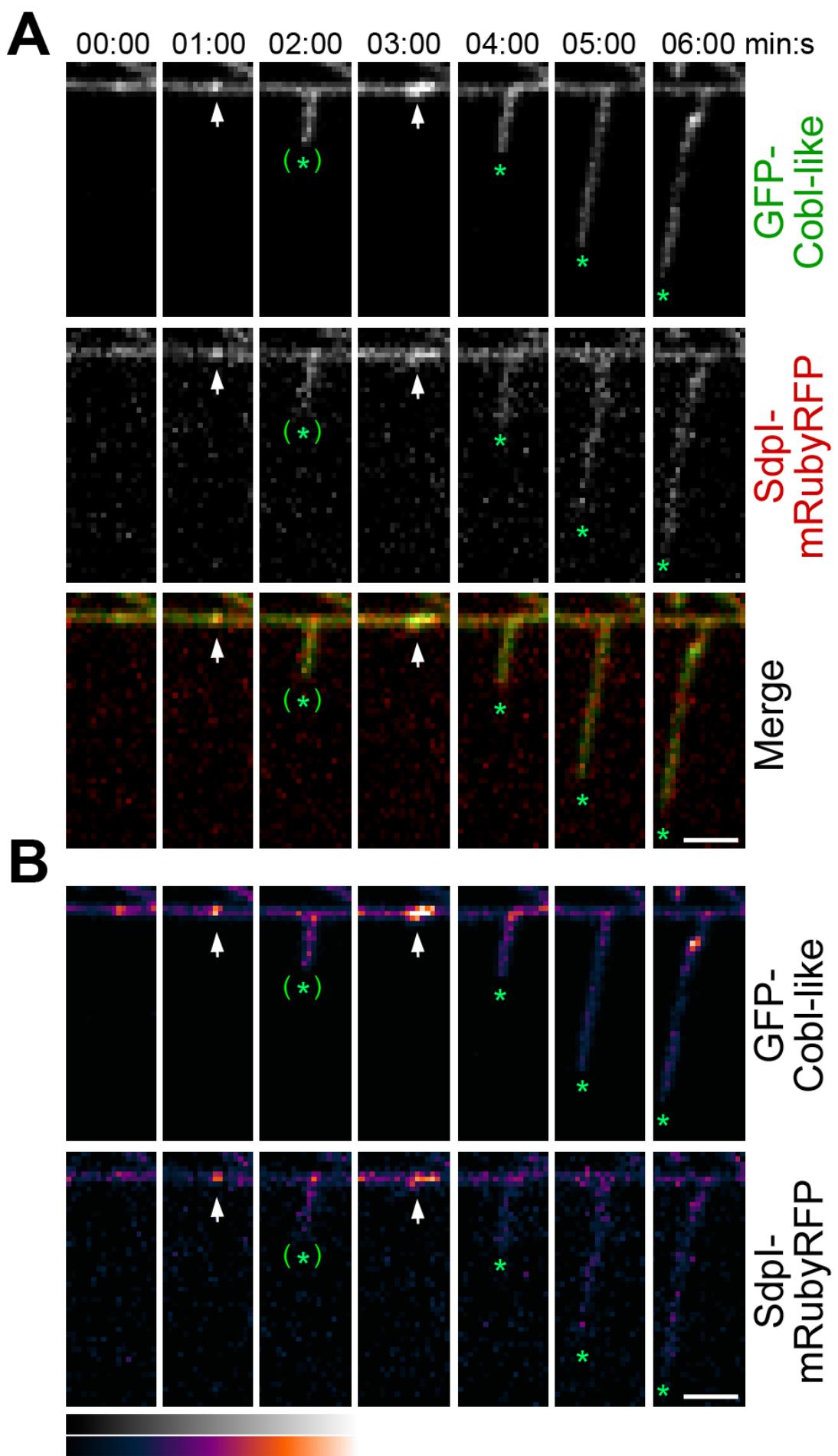
Figure 7
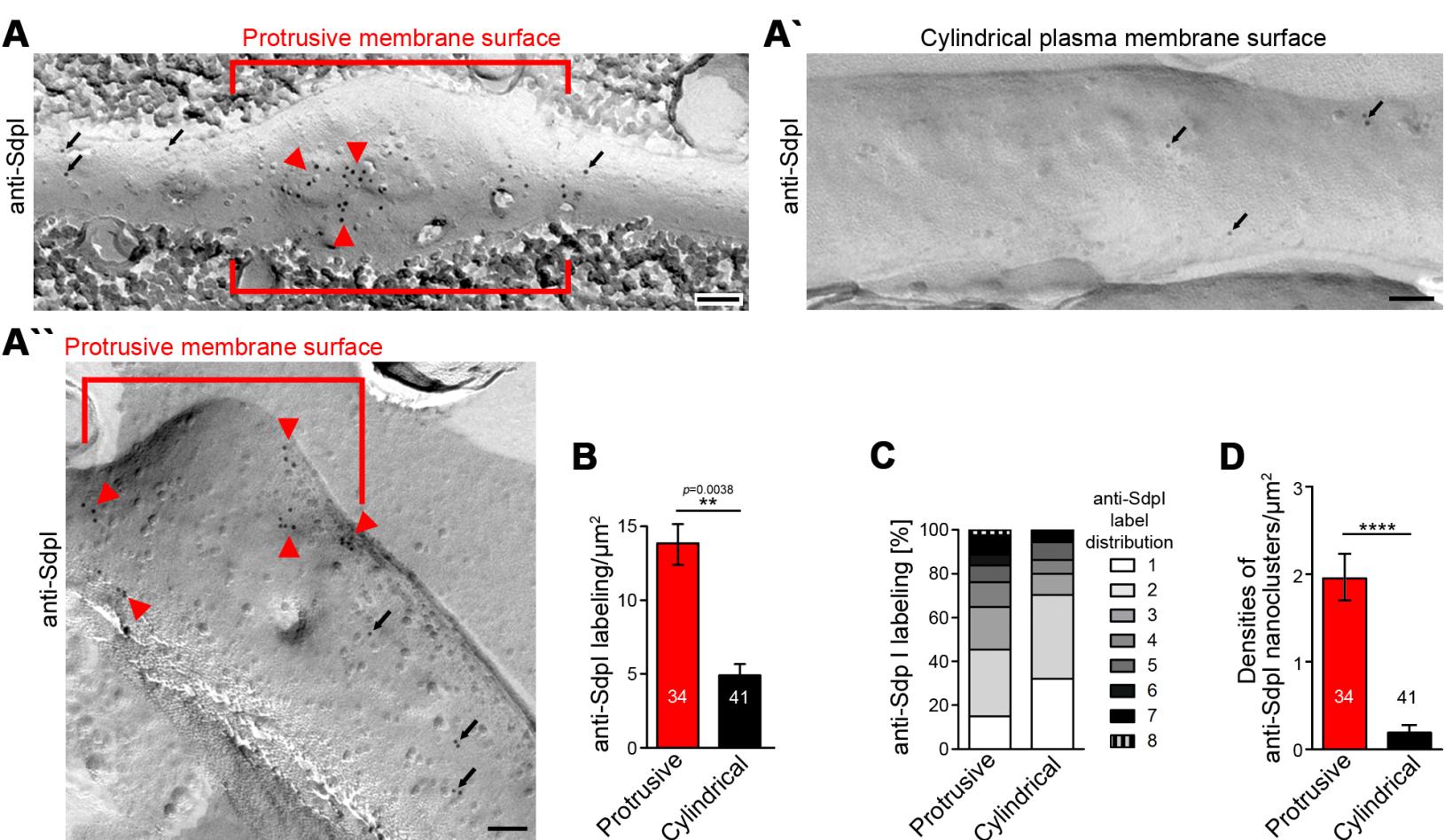
Figure 8
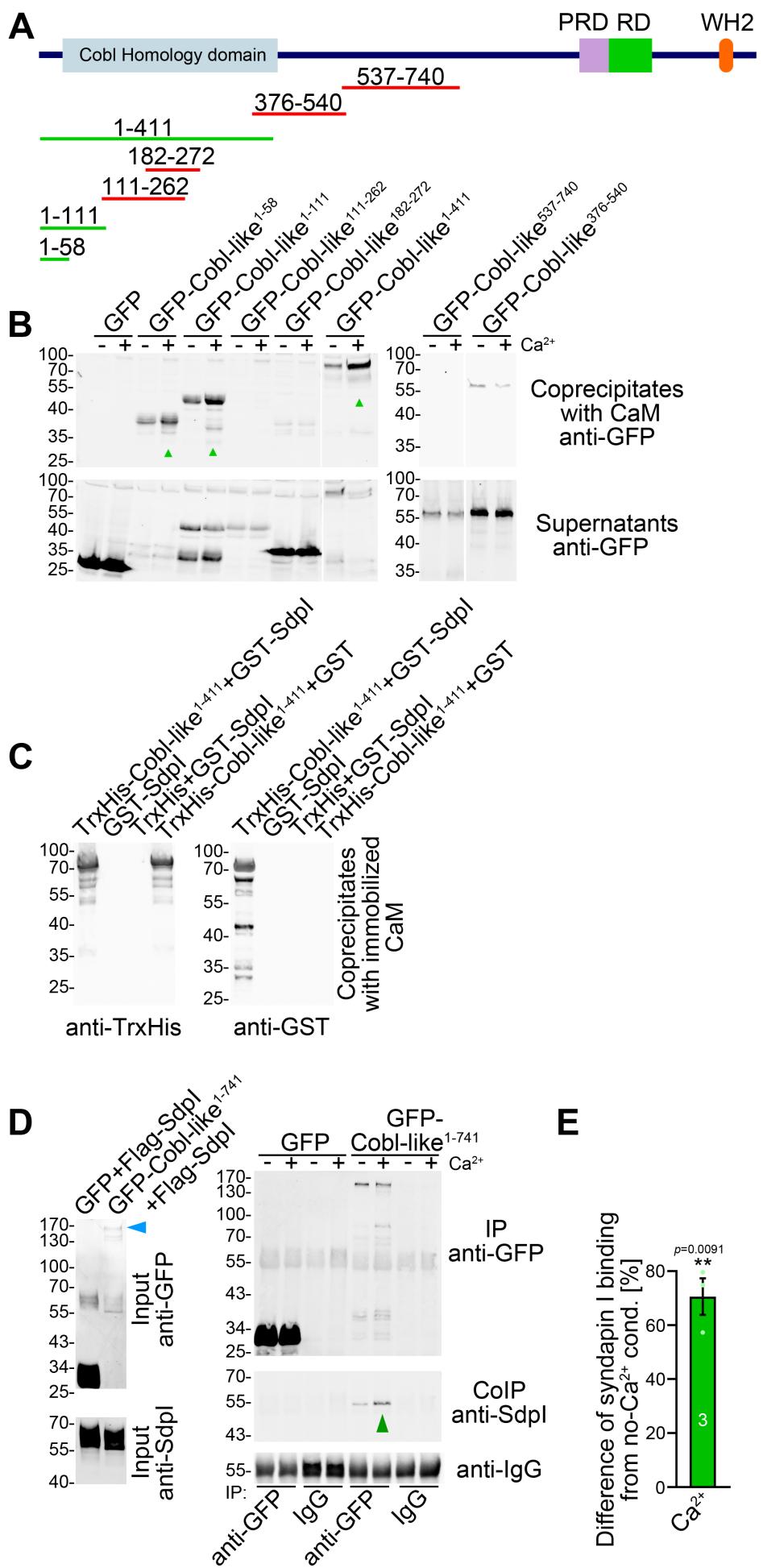
Figure 9
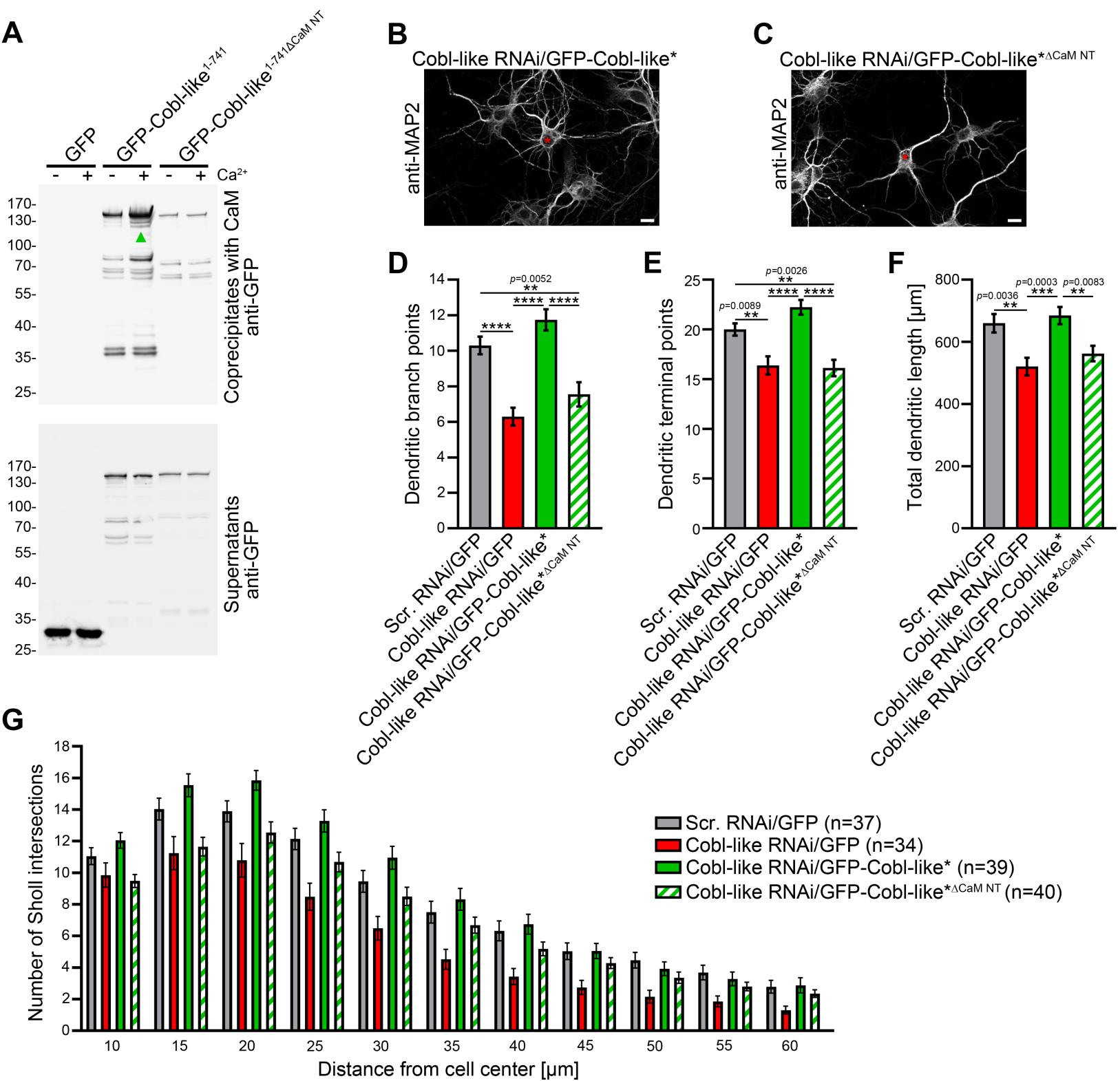
|	10	15	20	25	30	35	40	45	50
Scr. RNAi/GFP vs. Cobl-like RNAi/GFP	ns	** p=0.0012	*** p=0.0002	****	*** p=0.0004	*** p=0.0004	*** p=0.0007	* p=0.0131	* p=0.0125
Scr. RNAi/GFP vs. Cobl-like RNAi/GFP-Cobl-like*	ns	ns	* p=0.0411	ns	ns	ns	ns	ns	ns
Scr. RNAi/GFP vs. Cobl-like RNAi/GFP-Cobl-like*ΔCaM NT	ns	** p=0.0058	ns	ns	ns	ns	ns	ns	ns
Cobl-like RNAi/GFP vs. Cobl-like RNAi/GFP-Cobl-like*	* p=0.018	****	****	****	****	****	****	* p=0.0105	ns
Cobl-like RNAi/GFP vs. Cobl-like RNAi/GFP-Cobl-like*ΔCaM NT	ns	ns	ns	* p=0.017	* p=0.0367	* p=0.0203	ns	ns	ns
Cobl-like RNAi/GFP-Cobl-like* vs. Cobl-like RNAi/GFP-Cobl-like*ΔCaM NT	** p=0.0018	****	****	** p=0.0015	** p=0.0034	ns	ns	ns	ns

Figure 10

Figure 10–figure supplement 1

Figure 11

Cobl functions →

Dendritic branch induction

← **Cobl-like functions**

- Cobl-like deficiency

Cobl

F-actin

Ca²⁺

Syndapin I

Cobl-like

- Cobl deficiency

- Syndapin I deficiency

- Cobl-like loss-of-function
- Deletion of entire NT
- Disruption of N terminal CaM binding
- Disruption of syndapin I binding
- Disruption of syndapin I binding
  to CaM-regulated KRAP1

⭐ CaM

❙ WH2 domains

● KRAP motifs

✦ CaM-regulated KRAP1

● Syndapin SH3 domain